Project Final Report

Grant Agreement Number: FP7 - 285098

Project acronym: SOLAR-JET

Project title: **S**olar chemical demonstration and **O**ptimization for **L**ong-term **A**vailability of **R**enewable **JET** fuel

Funding Scheme: Collaborative Project (Small or medium-scale focused research project)

Name, title and organisation of the scientific representative of the project's coordinator:

Dr Andreas Sizmann,
Bauhaus Luftfahrt e.V.(BHL),
Willy-Messerschmitt-Straße 1,
85521 Ottobrun, Germany

Tel: +49 89 307 4849-38

Fax: +49 89 307 4849-20

E-mail: andreas.sizmann@bauhaus-luftfahrt.net

Table of Contents

List of Figures

List of Tables

1. Final Publishable Summary Report

Solar chemical demonstration and
Optimization for
Long-term
Availability of
Renewable
JET fuel

1.1 Executive Summary

With the first-ever production of synthesized “solar” jet fuel, the SOLAR-JET project has successfully demonstrated the entire production chain for renewable kerosene obtained directly from sunlight, water and carbon dioxide (CO_2), therein potentially revolutionizing the future of aviation. The project demonstrated an innovative process technology using concentrated sunlight to convert carbon dioxide and water to a so-called synthesis gas (syngas). This is accomplished by means of a redox cycle with metal-oxide based materials at high temperatures. The syngas, a mixture of hydrogen and carbon monoxide, is finally converted into kerosene by using commercial Fischer-Tropsch technology.

In the ETH laboratories, the reactive material was developed over the project period to obtain a dual-scale porosity which allows enhanced heat and mass transfer. It was also shown that the H_2/CO-ratio can be chosen to have the desired value for the Fischer-Tropsch conversion which obviates further species adjustments. A record solar thermochemical energy conversion efficiency of 1.7% was achieved with the first generation of the reactors used in the project. In a further development, a second generation of the reactor features a different geometry with improved temperature distribution in the reactive material and achieves an even higher energy conversion efficiency of unprecedented 2.7%.

Accompanying the experimental demonstration, a computational model was created at DLR which is able to describe accurately the behavior of the solar reactor. The model was validated with actual experimental data from the laboratory and provides a valuable tool to gain further insight into the heat and mass transfer characteristics. It is further used to model a scale-up of the reactor to a power input of 50 kWth.

In a dedicated analysis, the ecological and economic performance of the SOLAR-JET fuel pathway was assessed. It was found that for a baseline case plant with a capacity of 1000 barrels per day (bpd) of jet fuel and 865 bpd of naphtha, greenhouse gas emissions of 0.5 kg CO_2-equivalent/L jet

fuel at production costs of 2.2 €/L jet fuel are to be expected. Important drivers for both the ecological and economic performance were identified to be the thermochemical energy conversion efficiency and the solar resource. Further, a significant reduction of greenhouse gas emissions can only be expected if CO_2 is captured from a renewable, non-fossil source such as the atmosphere. Equally, using renewable instead of grid electricity is essential to achieve an excellent ecological performance due to its impact on life-cycle emissions.

A technological assessment revealed that most process steps are already used on an industrial scale, such as water desalination, concentration of solar energy, gas storage, and Fischer-Tropsch conversion. Further research and development is foremost required for the thermochemical conversion and CO2 capture from air. For the developed process steps, primarily cost targets apply, while for the other processes efficiency and/or cost targets have to be considered.

1.2 Context and Objectives

The EU Directive 2009/28/EC requires a 10% share of renewable energy in the transport sector in every Member State by 2020 and the EU energy roadmap for 2050 aims at a 75% share of renewables in the gross energy consumption. Achieving these targets requires a significant share of alternative transportation fuels, including a 40% target share of low carbon sustainable fuels in aviation[1]. Current biofuel technologies do not meet sustainability and availability requirements at the scale of future global fuel demand[2].

Converting solar energy into fuels has the potential of adding significant renewable capacity to the *European transport fuel mix*. Solar energy utilization is undisputedly scalable to any future demand and is already utilized at large scale to produce heat and electricity via solar-thermal and photovoltaic installations. Solar energy may also be used to produce hydrogen. However, specific transportation sectors cannot easily replace hydrocarbon fuels, with aviation being the most notable example. All current aircraft developments are designed for conventional jet fuel, since liquid hydrocarbons are ideal energy carriers with exceptionally high energy density and most convenient handling properties, and also because of the existing massive global infrastructure and because of the compatibility with conventional aircraft fuel systems. Due to long design and service times of aircrafts the aviation sector will critically depend on the availability of liquid hydrocarbons for decades to come[3]. Heavy duty trucks, maritime and road transportation are also expected to rely

[1] WHITE PAPER *Roadmap to a Single European Transport Area – Towards a competitive and resource efficient transport system* COM/2011/0144, doi:10.2832/30955, European Union 2011

[2] A. Mohr and S. Raman, *Lessons from first generation biofuels and implications for the sustainability appraisal of second generation biofuels.* Energy Policy **63**, 114, 2013; S. Y. Searle and C.J. Malins, *A Policy-Oriented Reassessment of Bioenergy Potential Estimates*. Proceedings of the 20th European Biomass Conference and Exhibition, Milan, 53, 2012, and references therein.

[3] Strategic Research & Innovation Agenda, **1** , 19, 2012; Advisory Council for Aviation Research and Innovation in Europe (ACARE)

strongly on liquid hydrocarbon fuels[4]. Thus, the large volume availability of 'drop-in' capable renewable fuels is of great importance for decarbonizing the transport sector.

Solar fuel path

The SOLAR-JET approach uses concentrated solar energy to synthesize liquid hydrocarbon fuels from H_2O and CO_2. This reversal of combustion is accomplished via a high-temperature thermochemical cycle based on metal oxide redox reactions which convert H_2O and CO_2 into energy-rich synthesis gas (syngas), a mixture of mainly H_2 and CO[5]. This two-step cycle for splitting H_2O and CO_2 is schematically shown in Figure 1 and represented by:

1st step, reduction $$MO_{ox} \rightarrow MO_{red} + \frac{1}{2}O_2$$

2nd step, oxidation with H_2O $$MO_{red} + H_2O \rightarrow MO_{ox} + H_2$$

2nd step, oxidation with CO_2 $$MO_{red} + CO_2 \rightarrow MO_{ox} + CO$$

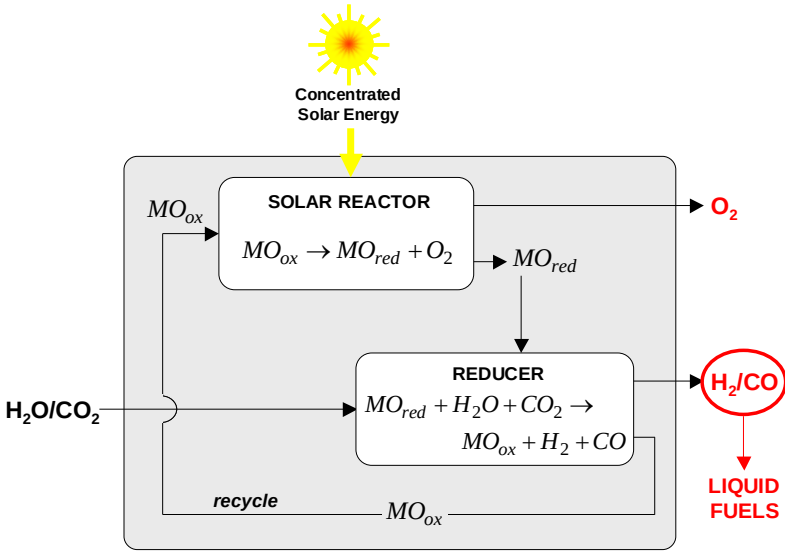

Figure 1: Schematic of a two-step solar thermochemical cycle for H_2O/CO_2 splitting based on metal oxide redox reactions. MO_{ox} denotes a metal oxide, and MO_{red} the corresponding reduced metal or lower-valence metal oxide. In the first, endothermic, solar step, MO_{ox} is thermally dissociated into MO_{red} and oxygen. Concentrated solar radiation is the energy source for the required high-temperature process heat. In the second step, MO_{red} reacts with H_2O/CO_2 to produce H_2/CO (syngas). The resulting MO_{ox} is then recycled back to the first step, while syngas is further processed to liquid hydrocarbon fuels[5].

The first, endothermic step is the solar thermal reduction of the metal oxide MO_{ox} to a lower-valence metal oxide MO_{red}. The second, non-solar, exothermic step is the reaction of the reduced metal oxide with H_2O or CO_2 to form H_2 or CO, and reform the original metal oxide which is recycled to the first step. The net reactions are $H_2O \leftrightarrow H_2+½O_2$ and/or $CO_2 \leftrightarrow CO+½O_2$. Since

[4] IEA, *World Energy Outlook 2013*

[5] M. Romero and A. Steinfeld, *Concentrating Solar Thermal Power and Thermochemical Fuels*, Energy Environ. Science, **5**, 9234, 2012

H_2/CO and O_2 are formed in different steps, the problematic high-temperature fuel/O_2 separation is thereby eliminated. The net product is high-quality synthesis gas (syngas), which is further processed to energy-dense, liquid hydrocarbons via Fischer-Tropsch (FT) synthesis. FT synthetic paraffinic kerosene derived from syngas is already certified for aviation.

SOLAR-JET fuels are most efficiently and competitively produced in desert regions with high direct normal solar irradiation (DNI, typically > 2000 kWh·m^{-2} per year), thus there is no land competition with food or feed production (Figure 2). In contrast to current alternative fuels, solar fuels can easily meet future fuel demand by utilizing less than 1% of the global arid and semi-arid land[6]. High area-specific yields result in a very small environmental impact from direct or indirect land-use change (Figure 3).

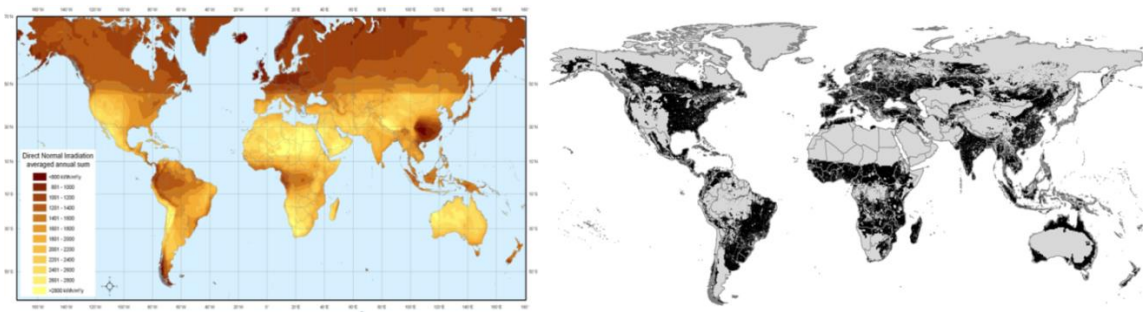

Figure 2:* Direct solar irradiation (left) and available global agricultural area (right)[7]*. Suitable regions for solar fuel production do not compete for land with food and feed production. For solar fuels, less then 1% of the arid and semi-arid land are sufficient to meet global fuel demand. Solar fuels add great capacity to the renewable fuel portfolio and enable regional diversification, as areas for biofuel and solar fuel production barely overlap.

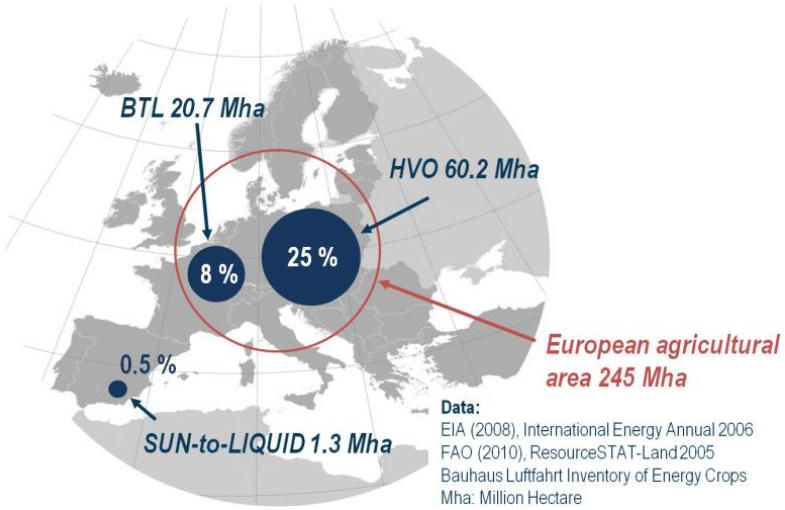

Figure 3: Area required for the complete substitution (100%) of European jet fuel demand (Turkey included, CIS states excluded) normalized to the European agricultural area (2005 baseline). The high specific yield of solar fuels arises from a favourable solar-to-fuel energy

[6] F. Trieb et al., *Global Potential of Concentrating Solar Power*, SolarPaces Conference, Berlin 2009 (adopted to solar fuel production)

[7] Sources: Available global agricultural area, Bauhaus Luftfahrt GIS-based Assessment; Direct Normal Irradiance: DLR

conversion efficiency and from the large solar resource at suitable locations. Assumed yields: HVO: (Hydrotreated Vegetable Oil), rapeseed, annual specific yield 1115 l/ha. BTL: (Biomass-to-Liquid), short rotation woody biomass, annual specific yield 3240 l/ha SUN-to-LIQUID fuel (such as SOLAR-JET): Annual specific yield 50.000 l/ha (10% solar-to-fuel energy conversion efficiency, 25% area coverage by concentrating system, annual direct normal irradiance 2000 kWh/m^2).

Objectives

The primary objectives of the SOLAR-JET project are.

- Technological potential of solar kerosene
- Solar chemical reactor design and fabrication
- Production of “solar” kerosene
- Testing in a solar simulator facility
- Solar chemical reactor modelling
- Further technology requirements and an economic assessment

The primary objective are explained in detail in the following:

Technological potential of solar kerosene

The comparison of SOLAR-JET fuel with other alternative fuels and fossil kerosene with respect to life-cycle efficiency, CO_2 emissions and yield requires a well-defined quantitative assessment framework. This framework defines metrics and methods, assumptions and information sources for calculating transparent, objective and reproducible figures of merit. This framework allows a comparison of the SOLAR-JET performance indicators with the state of the art during the project to be made, to estimate the substitution potential of kerosene and to identify criticalities in the solar fuel production chain which need to be addressed in the project or in an R&D roadmap beyond the scope of SOLAR-JET.

Solar chemical reactor design and fabrication

A solar chemical reactor is designed and fabricated to realize the two-step solar thermochemical cycle based on non-stoichiometric ceria redox reactions for producing syngas from H_2O and CO_2. The design incorporates results from the modeling of different geometries with coupled heat transfer and chemical reactions to achieve higher solar-to-fuel efficiencies and yields and specific CO/H_2 syngas ratios. The technology gaps are identified and addressed throughout the process.

Production of kerosene

The first “solar” aviation fuel is produced. The close collaboration between units delivering the starting product (syngas) and those synthesizing the jet fuel (both are represented in this project) allows adapting processes for achieving highest yield and efficiency. Moreover, technological gaps (e.g. using the Fischer-Tropsch process with solar-synthesized syngas) are addressed. Outcomes

are then translated into a technological advance for all participants and (by means of dissemination activities) to interested partners currently not part of project.

Testing in a solar simulator facility

Experimentation is performed for the non-optimized and the optimized solar chemical reactors in the high-flux solar simulator (HFSS) at ETHZ. The HFSS provides an external source of intense thermal radiation, mostly in the visible and IR spectra that closely approximates the heat transfer characteristics of highly concentrating solar systems, such as solar towers and dishes. Power heat fluxes are adjustable by the number of Xe arcs in operation, the position of the venetian shutter, and the position of the test target relative to the focal plane. This provides an ideal environment for experimentation under controlled, repeatable conditions. Various parameters are identified and varied throughout the experimental campaigns to optimize efficiencies, yields, and CO/H_2 ratios of the syngas. The results are provided to the modellers for validation and disseminated in high impact, peer-reviewed journal publications and at international conferences.

Solar chemical reactor modelling

Within the scope of the project detailed modelling capabilities of heat transfer coupled with chemical reactions are developed and tested. They enable partners (and the engineering community by means dissemination activities) to investigate and optimize this new technology. Reliable predictions of key parameters such as reactor yield, overall efficiency and CO/H_2 ratio are verified. The numerical tools are then used to investigate different reactor geometries and finding device scaling rules, a key parameter for the assessment of the technology potential and further needed technological improvements.

Further technology requirements and an economic assessment

With the combined expertise of all partners, a high-level case analysis of SOLAR-JET, commensurate with the inherent uncertainty of turning scientific advancements into technological innovation and commercial success is presented. The synthesizing work of the SOLAR-JET approach integrates the theoretical and experimental results into a clear and transparent representation of the potential impact on and advancements of future alternative fuel technology and economics for aviation.

As a result, a better understanding of the technologies and economics of scaling up the SOLAR-JET fuel production, the R&D requirements and potential benefits and risks is obtained and a first roadmap for resolving the identified most important issues for implementation is presented.

1.3 Main Results / Foreground

Syngas production by simultaneous splitting of CO_2 and H_2O

Initial experimental work with the solar reactor focused on the assessment of simultaneous splitting of

CO_2 and H_2O to co-produce a mixture of CO and H_2 (syngas) with the desired molar ratio of H_2:CO suitable for the subsequent catalytic conversion to jet fuel via FT-synthesis. The co-feeding molar ratio H_2O:CO_2 was varied to examine its influence on the H_2:CO molar ratio. Consecutive splitting cycles were performed to assess cyclability.

Figure 4 shows the H_2:CO molar ratio of the syngas produced as a function of the H_2O:CO_2 molar ratio of the reacting gas mixture. The H_2:CO molar ratio increased linearly from 0.25 to 2.34 for H_2O:CO_2 molar ratios varying from 0.8 to 7.7. According to these results, co-feeding with H_2O:CO_2 = 5.6 yields syngas with H_2:CO = 1.7, which is suitable for the processing of liquid fuels (e.g. diesel, kerosene) via low-temperature Fischer-Tropsch.

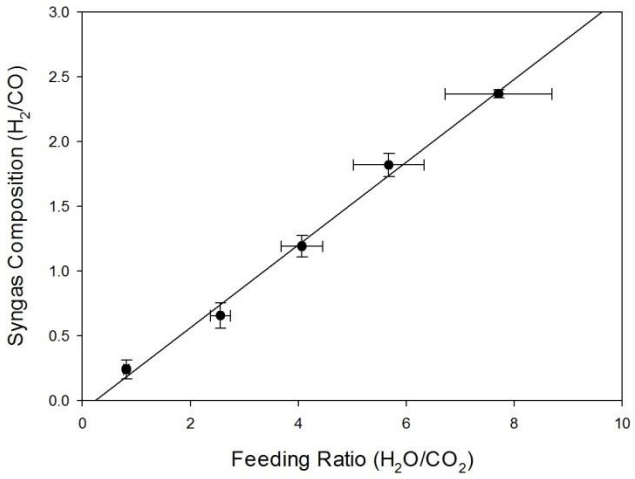

Figure 4: H_2:CO molar ratio of the syngas produced as a function of the H_2O:CO_2 molar ratio of the reacting gas mixture. Error bars in x-direction indicate the error of the flow controllers, error bars in y-direction indicate the standard deviation from the experimentally measured and averaged composition.

Figure 5 shows ten consecutive H_2O/CO_2 splitting cycles performed over 8 hours at a constant feeding ratio (H_2O:CO_2= 6.7), yielding syngas with an average H_2:CO ratio of 2.36 ± 0.07. Consistent with single cycle experiments, production of syngas was immediately observed after injection of the H_2O/CO_2 mixture, reaching an average peak rate of 0.48 ± 0.08 ml min^{-1} g^{-1} CeO_2 (H_2: 0.32 ± 0.06 ml min^{-1} g^{-1} CeO_2, CO: 0.16 ± 0.03 ml min^{-1} g^{-1} CeO_2) , an average rate of 0.2 ± 0.01 ml min^{-1} g^{-1} CeO_2 (H_2: 0.14 ± 0.03 ml min^{-1} g^{-1} CeO_2, CO: 0.06 ± 0.01 ml min^{-1} g^{-1} CeO_2), and a total fuel production of 3.15 ± 0.49 ml g^{-1} CeO_2 (H_2: 2.21 ± 0.34 ml g^{-1} CeO_2, CO: 0.94 ± 0.15 ml g^{-1} CeO_2).

Figure 5:

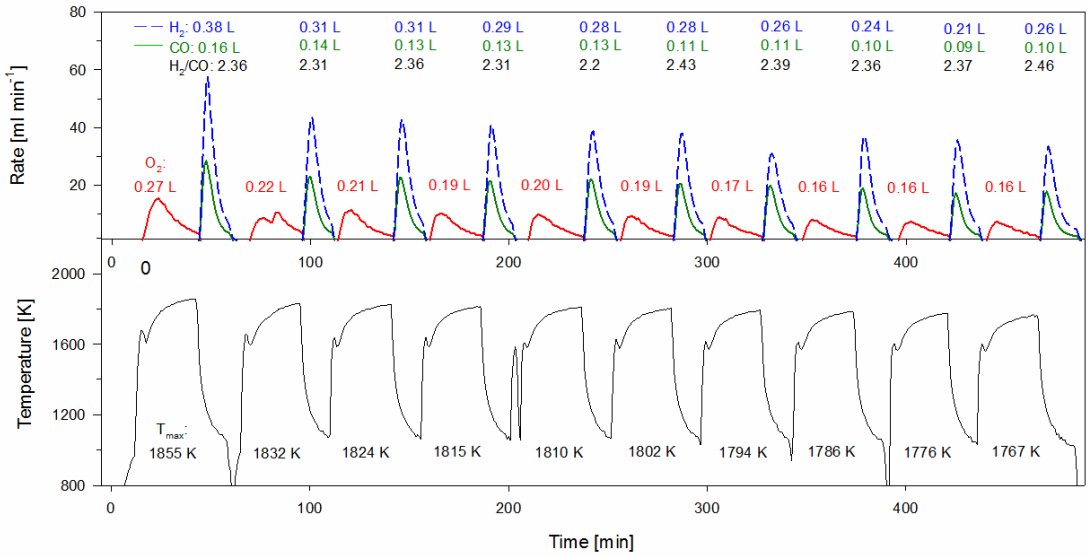

Temperature of the ceria felt, gas production rates, total amount of evolved gases, and H_2:CO molar ratios during ten consecutive splitting cycles. Experimental conditions: 3.6 and 0.8 kW radiation power input during reduction and oxidation steps, respectively; 2 l/min Ar purge gas during both reduction and oxidation steps; 2.2 l/min H_2O and 0.33 l/min CO_2 during the oxidation step (H_2O:CO_2 molar ratio of 6.7). The reduction and oxidation steps were performed at constant time intervals of 30 and 15 minutes, respectively.

Optimized solid reactant

The H_2O/CO_2 co-feeding experiments indicated that both the solar-to-fuel energy conversion efficiency and the cycling rates were limited largely by the low radiative heat transfer rates achieved with opaque structures, such as ceria felt, leading to undesired temperature gradients across the structure and long heating times. Therefore, a novel reticulated porous ceramic (RPC) foam made of pure CeO_2 was developed and experimentally assessed for thermochemical redox cycling in the SOLARJET reactor. The ceria-made RPC acts as the reactive material itself and inherently combines the advantages of volumetric radiation absorption, rapid reaction rates, and high mass loading of reactive material. This ultimately results in experimentally measured efficiency values and fuel production rates that are significantly higher than those previously reported. Figure 6 shows photographs of the fabricated ceria RPC parts for the solar cavity receiver.

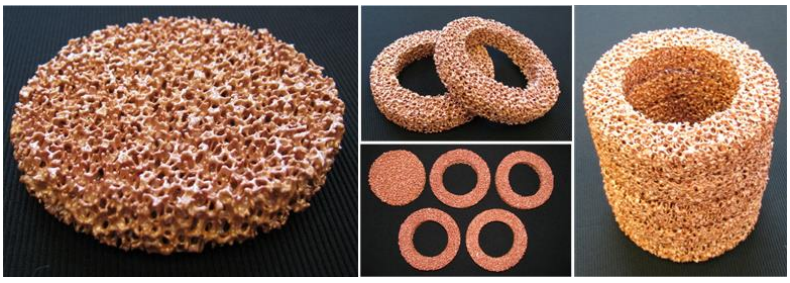

Figure 6: CeO_2 RPC parts fabricated for the solar cavity-receiver. One set consists of a disk (20 mm thickness, 100 mm OD) and four rings (20mm thickness, 60 mm ID, 100 mm OD).

The advantage of the macro-structured RPC vis-à-vis the micro-structured felt (both made of pure ceria) is seen clearly when comparing experimental results using the same solar reactor under same operating conditions. Figure 7 shows the specific – per unit mass of ceria – and absolute production

rates of O_2 during the reduction step and of CO during the oxidation step obtained with RPC (left) and felt (right graphs). The experimental conditions for both structures were: 3.4 kW solar radiative power input and 2 l min^{-1} Ar during the reduction step, and 0.8 kW solar radiative power input and 3 l min^{-1} CO_2 + 2 l min^{-1} Ar during the oxidation step. The specific amounts and rates of O_2 released per gram CeO_2 are comparable for both structures, but the absolute values are much greater for the RPC (4.00 l) than for the felt (0.24 l). This is partly due to the fact that the bulk density of the RPC is larger and more mass could fit into the reactor (1413 g for RPC vs. 90 g for felt). However, more mass loading that is not uniformly heated to the reduction temperature would have a detrimental effect on $\eta_{\text{solar-to-fuel}}$ because more solar energy would be "wasted" on heating unreacted material. Thus, the main cause for the superior performance of the RPC as compared to the felt is linked to heat transfer. The macro-pore structure of the RPC enabled deeper penetration and volumetric absorption of concentrated solar radiation, as aforementioned discussed, which in turn resulted in a more uniform temperature distribution and prevented overheating of the surfaces directly exposed to the high-flux irradiation. In contrast, the micro-pore structures of felts or monolithic bricks (μm range pore size) were optically thicker to the solar spectrum and absorbed the impinging radiation primarily on the exposed innermost surface of the cylinder, causing larger temperature gradients across the thickness of the structure and, consequently, restraining the reaction to the innermost layers only. SEM micrographs of the felt after the experiments corroborated the large temperature gradient as significant sintering was detected in the innermost layers exposed to the high-flux irradiation but negligible sintering occurred in the outer layers.[1] This thesis is further supported by radiative heat transfer analysis of the RPC and monolithic bricks via Monte Carlo ray-tracing at the pore-scale on the exact 3D digital geometry obtained by computer tomography.[2,3] Within the limits of the numerical truncation error (i.e., mesh refinement) and the accuracy of geometrical representation (i.e., tomography resolution), the results obtained by this methodology approached the exact solutions. Mean values of the effective extinction coefficient obtained were 280 m^{-1} for the RPC and 40,000 m^{-1} for the monolith bricks, indicating a two orders of magnitude higher optical thickness for the latter.

During the oxidation step, the RPC and felt structures exhibited substantially different temporal behaviour. For the felt, a rapid increase in the CO rate was followed by an exponential decline and completion of the reaction after a short period of time. For the RPC, the CO evolution proceeded at considerably slower rate and was characterized by a bell shaped curve with a long tale. Peak reaction rates, normalized by the mass of ceria, were about 9 times lower for the RPC (RPC: 0.33 ± 0.01 ml min^{-1} g^{-1} CeO_2 ; felt: 2.85 ± 0.13 ml min^{-1} g^{-1} CeO_2). The complete oxidation took more than 4 times longer for the RPC (RPC: 60 min; felt: 14 min). This behaviour is attributed to the fact that the oxidation rate is mainly controlled by the availability of reactive surface exposed to CO_2.[4] BET measurements (TriStar 3000, Micromeritics) indicated specific surface areas of 6.0 m^2 g^{-1} for the felt and less than 0.1 m^2 g^{-1} (detectable limit) for the RPC. Based on tomographic scans, a specific surface area of $1.45 \cdot 10^{-4}$ m^2 g^{-1} was determined for the RPC. Nevertheless, the absolute CO production with the RPC (8.27 l) was nearly 17 times that of the felt (0.49 l) because of the higher mass loading, which was 15.7 times that of the felt.

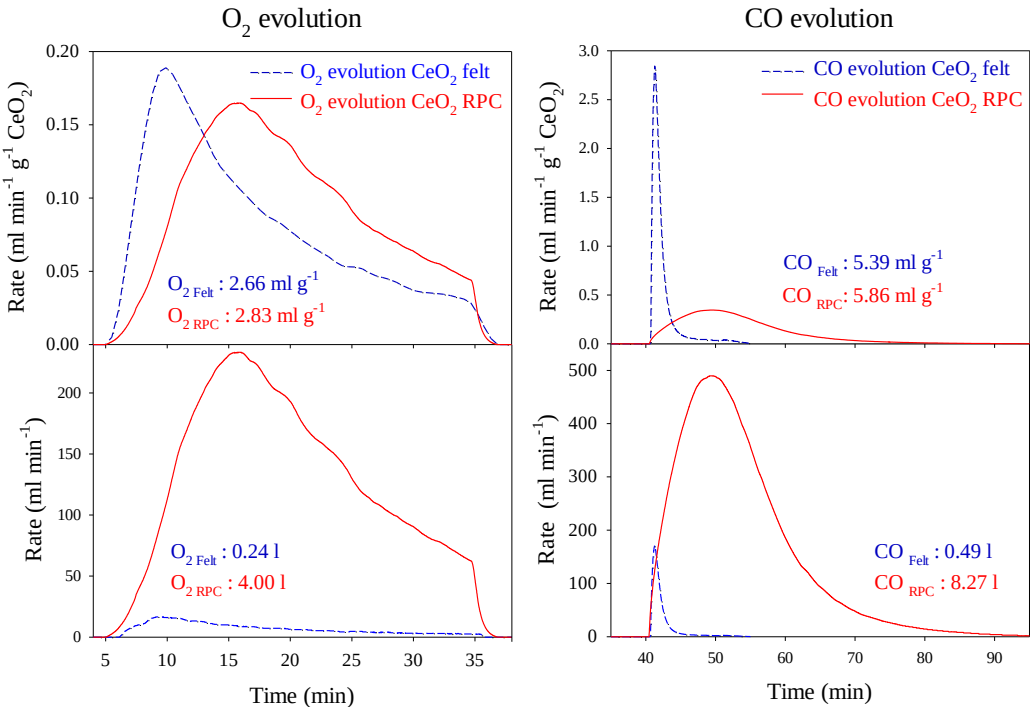

Figure 7: Specific (upper graphs) and absolute (lower graphs) production rates of O_2 during the reduction step and of CO during the oxidation step obtained with RPC (left graphs; this study) and felt (right graphs). Experimental conditions: 3.4 kW solar radiative power input and 2 l min^{-1} Ar during the reduction step; 0.8 kW solar radiative power input and 3 l min^{-1} CO_2 + 2 l min^{-1} Ar during the oxidation step. Sample mass: 1413 g for RPC, 90 g for felt.

Average and peak solar-to-fuel energy conversion efficiencies are defined as:

$$\eta_{\text{solar-to-fuel, average}} = \frac{\Delta H_{\text{CO}} \int r_{\text{CO}}\, dt}{\int P_{\text{solar}}\, dt + E_{\text{inert}} \int r_{\text{inert}}\, dt} \quad (1)$$

$$\eta_{\text{solar-to-fuel, peak}} = \frac{2 r_{\text{oxygen}}\, \Delta H_{\text{CO}}}{P_{\text{solar}} + r_{\text{inert}}\, E_{\text{inert}}} \quad (2)$$

where r_{CO} is the molar rate of CO production during oxidation, r_{oxygen} is the molar rate of O_2 evolution during reduction, ΔH_{CO} is the heating value of CO, P_{solar} is the solar radiative power input, r_{inert} is the flow rate of the inert gas during reduction, and E_{inert} is the energy required to separate the inert gas (assumed 20 kJ mol^{-1}).[5] $\eta_{\text{solar-to-fuel, average}}$ is calculated by integration of the CO production and energy consumption over the complete redox cycle. It also accounts for the solar energy needed to re-heat the reactants up to the reduction temperature. This is because the solar reactor is cool-down and re-heated between the redox steps during cyclic operation. Therefore, integration of P_{solar} (Eq. 1) accounts for the required re-heating once the oxidation step is completed. The definition of $\eta_{\text{solar-to-fuel, average}}$ (Eq. 1) is valid regardless whether the process is being performed in a batch, continuous, or semi-batch/semi-continuous mode, since the integration is carried out for the duration of the complete cycle. In the present case, P_{solar} = 0 during the exothermic oxidation step. The use of P_{solar} without interruption can be accomplished by the operation of two solar reactors side-by-side, one undergoing oxidation while the other undergoing reduction, by switching the concentrated solar beam between the two reactors.[6] The

same applies for a single solar reactor in which the reactive solid material is transported from the reduction zone to the oxidation zone and vice-versa,[7] or for a single solar reactor used exclusively for the reduction step while the reduced metal oxide is transported to an external (non-solar) reactor for the oxidation step and recycled to the solar reactor.[8,9] On the other hand, $\eta_{\text{solar-to-fuel, peak}}$ is calculated based on the peak O_2 evolution rate attained during reduction assuming stoichiometric fuel production rate. This assumption is justified by closing the net mass balance for the complete cycle, i.e. $CO_2 = CO + ½ O_2$. The highest efficiency values achieved were $\eta_{\text{solar-to-fuel, average}}$ =1.73% and $\eta_{\text{solar-to-fuel, peak}}$ = 3.53% for a solar radiative power input of 3.8 kW. These are more than 4 times greater than the next highest efficiency reported in the literature for CO_2 conversion to CO using solar energy.[10,11,12,13] Previous experimental work performed in a similar solar reactor configuration with porous monolithic bricks resulted in $\eta_{\text{solar-to-fuel, average}}$ = 0.4 % and $\eta_{\text{solar-to-fuel, peak}}$ = 0.8 %.[11] Experiments performed on the simultaneous splitting of H_2O and CO_2 using porous ceria felt resulted in $\eta_{\text{solar-to-fuel, average}}$ = 0.15 % and $\eta_{\text{solar-to-fuel, peak}}$ = 0.31 %.[1] We attribute the higher values obtained in this work to a more efficient radiative heat transfer to the reactive material during the reduction step and the higher mass loading of CeO_2 inside the cavity.

Demonstration of the entire production chain to renewable kerosene via solar thermochemical splitting of H_2O and CO_2

The SOLARJET consortium has experimentally demonstrated in the framework of an extensive experimental campaign the first ever production of jet fuel via a thermochemical H_2O/CO_2-splitting cycle using simulated concentrated solar radiation. The key component of the production process of sustainable “solar kerosene” is the high-temperature solar reactor prototype which contains the optimized RPC structure made of pure CeO_2. The solar-to-fuel energy conversion efficiency was 1.72 %, without sensible heat recovery. A total of 291 stable redox cycles were performed, yielding 700 standard liters of syngas of composition 33.7 % H_2, 19.2 % CO, 30.5 % CO_2, 0.06 % O_2, 0.09 % CH_4, and 16.5 % Ar, which was compressed to 150 bars and further processed via Fischer-Tropsch synthesis to a mixture of naphtha, gasoil, and kerosene.

During the experimental campaign we examined in detail the cyclic performance of the 4 kW solar cavity-type reactor and assessed various operational aspects that are of particular importance when considering the process implementation on an industrial scale. Specifically, the augmentation of the reaction rates by the dual-scale RPC vis-à-vis the single-scale RPC is investigated by comparing CO_2-splitting redox cycles with the solar reactor under the same experimental conditions. The duration of the reduction and oxidation steps were optimized for maximizing the solar-to-fuel energy conversion efficiency. We further studied parametrically the fuel yield and composition during CO_2-splitting and simultaneous H_2O/CO_2-splitting by executing multiple consecutive redox cycles under varying experimental conditions of solar radiative power and reacting flow configurations. The stability of the dual-scale RPC and the cyclic performance of the solar reactor were evaluated by carrying out over 290 redox cycles under realistic operating conditions of direct high-flux irradiation and transient heat/mass transfer. The results provide compelling evidence for the technological viability of solar syngas

generation of desired stoichiometry from H_2O and CO_2. Finally, we experimentally showed the syngas-to-liquid process by compressing and storing of the produced syngas at 150 bar, and – without any composition adjustment – its further processing via FT-synthesis to naphtha, kerosene, and gasoil.

The schematic of the experimental setup is shown in Figure 8a) , and features the main system components of the production chain to solar kerosene from H_2O and CO_2 via the ceria-based thermochemical redox cycle. The key component is the solar reactor, shown schematically in Figure 8 b).

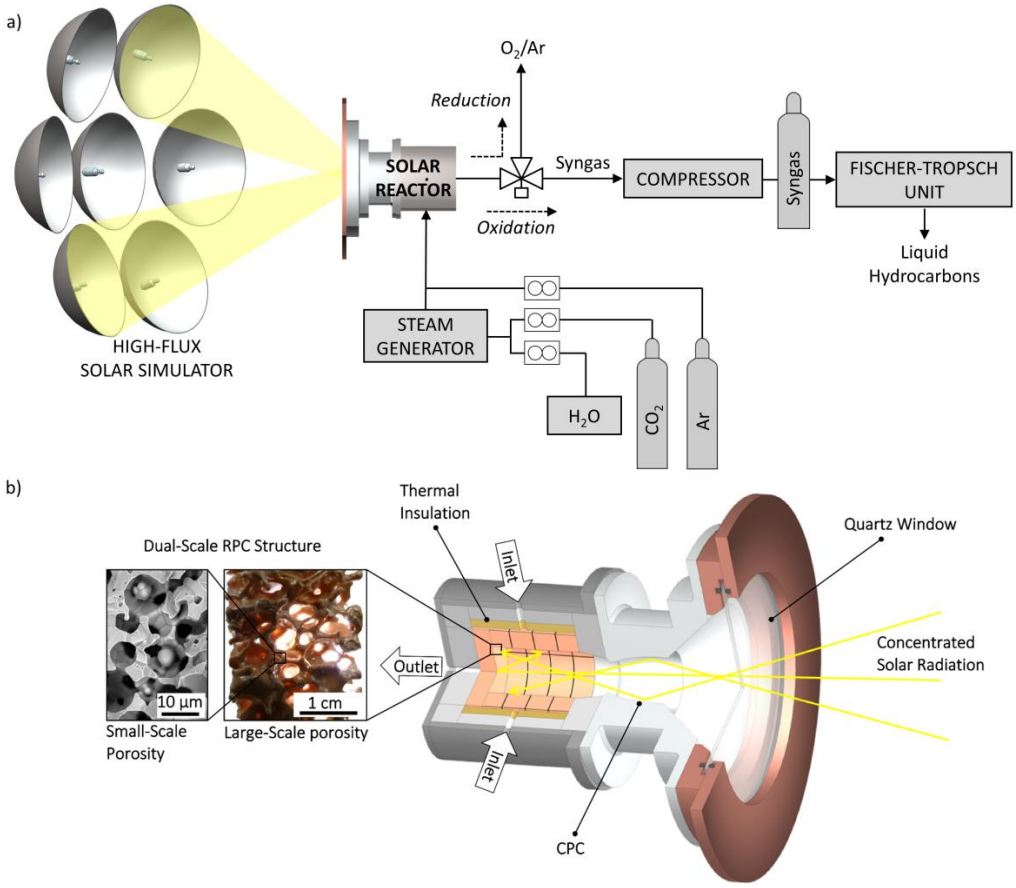

Figure 8: a) Schematic of the experimental setup, featuring the main system components of the production chain to solar kerosene from H_2O and CO_2 via the ceria-based thermochemical redox cycle. b) Schematic of the solar reactor configuration. The cavity-receiver contains a reticulated porous ceramic (RPC) structure, made from ceria, with dual-scale porosity in the mm- and µm-scale.

Figure 9 shows the nominal solar reactor temperature at the end of the reduction step and the peak CO and H_2 evolution rates for 291 redox cycles. The syngas produced during 243 cycles (regions III and IV of Figure 9) was collected and compressed into a 5 L standard aluminum gas bottle to a final pressure of 150 bar at room temperature. This corresponded to 700 standard liters of syngas with a final composition of 33.7 % H_2, 19.2 % CO, 30.5 % CO_2, 0.06 % O_2, 0.09 % CH_4, and 16.5 % Ar. Unreacted H_2O was condensed and separated. Adverse poisons for FT-catalysts were not detected at a lower detection limit (LOD) of 1 ppb by PTR-MS. The trace amount of O_2 was presumably due to O_2 still trapped in the pipes when switching from reduction to oxidation mode, while CH_4 was likely formed by methanation on catalytic metallic surfaces. The H_2:CO molar ratio was 1.76, which fits the targeted

syngas quality for FT-synthesis, proving the good controllability of the process. Traces of $Ni(CO)_4$ were detected downstream of the compressor station (but not at the exit of the solar reactor), indicating its formation by CO reacting with stainless steel piping at high pressures. Its formation can be simply avoided by using Ni-free components in the compression and storage unit.

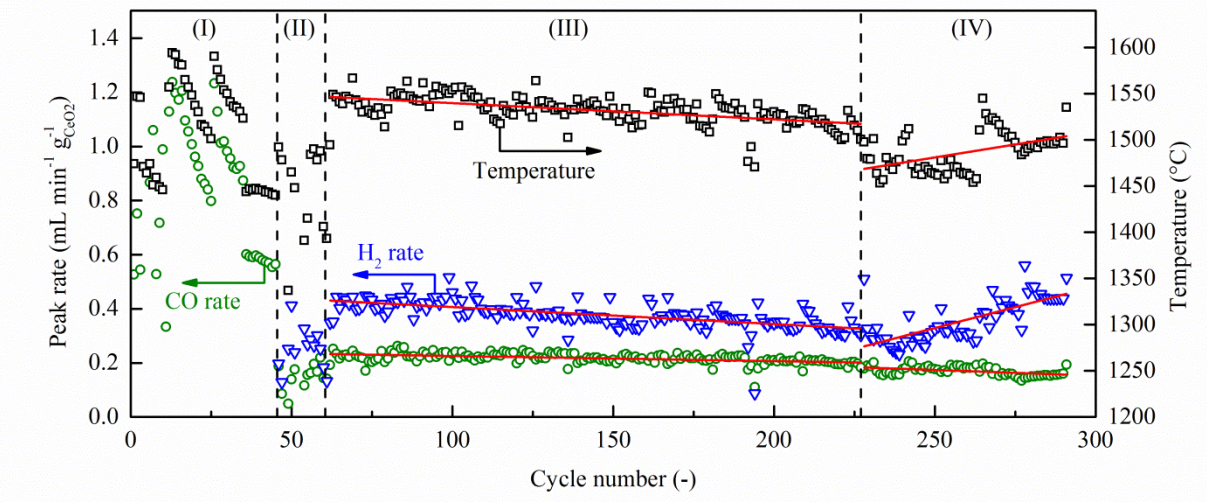

Figure 9: Nominal solar reactor temperature at the end of the reduction step and peak CO and H2 production rates versus cycle number for 291 redox cycles, measured with the solar reactor containing RPC.

Design and experimental assessment of a 2nd generation solar reactor prototype

Based on the experimental results with the first solar reactor prototype, a 2nd generation lab-scale reactor has been designed, fabricated and experimentally assessed at ETH. The geometry and flow configuration were determined based on Monte-Carlo ray tracing and CFD simulations performed at ETH with the aim of obtaining a more uniform flux distribution inside the cavity receiver and to avoid back-flow of gases from the cavity to the reactor front. Reticulated porous ceramic (RPC) structure made of ceria was used as the redox material. The complete experimental setup, consisting of the solar reactor, gas feeding and off-gas peripherals, and associated measurement & control instrumentation have been installed at the ETH's High-Flux Solar Simulator.

Reactor design

The main components of the 2nd-generation solar reactor are schematically shown in Figure 10. It consists of an insulated cavity-receiver with a 4 cm-diameter aperture for the access of concentrated solar radiation. The reactor front is sealed by an 11 cm-diameter, 4 mm-thick clear fused quartz disk window. The ceria RPC is contained within the cavity and consists of 8 bricks and 1 octagonal back plate to form an octagonal cavity with 100 mm-i.d., 150 mm-o.d. and 100 mm in height. The octagonal assembly was chosen to allow thermal and chemical expansion of the RPC parts without inducing extensive stress. Figure 11 a) and b) show photographs of the RPC reactor parts and the RPC's mounted in the solar reactor, respectively.

The geometry of the cavity was designed based on Monte-Carlo ray tracing simulations with the aim of obtaining a more uniform flux distribution over the irradiated RPC surface. Additional gas inlets behind

the aperture, depicted in Figure 12, were integrated to avoid back-flow of gases from the cavity to the reactor front to prevent condensation of sublimated ceria on the quartz window. A gas gap between the ceria RPC and the insulation ensures uniform flow of gases across the RPC. Figure 13 a) and b) show photographs of the solar reactor and the experimental setup at ETH's High-Flux Solar Simulator.

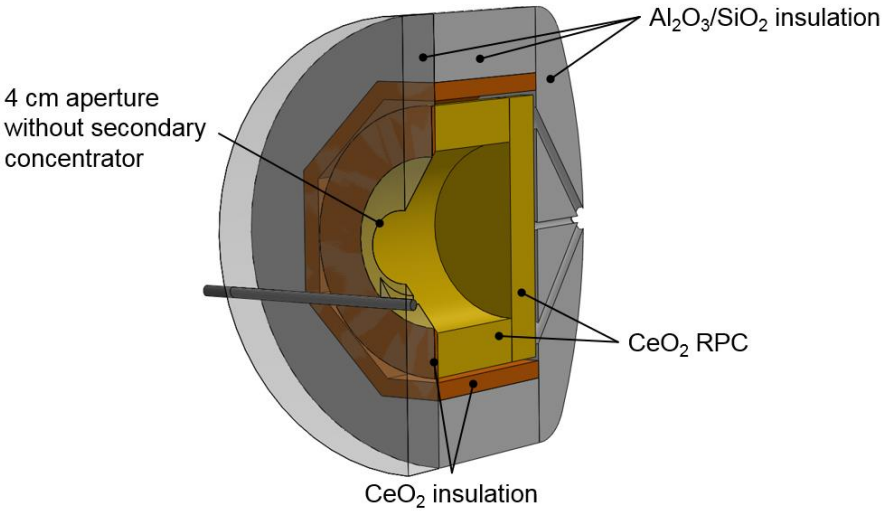

Figure 10: Configuration of the 2nd-generation solar reactor design

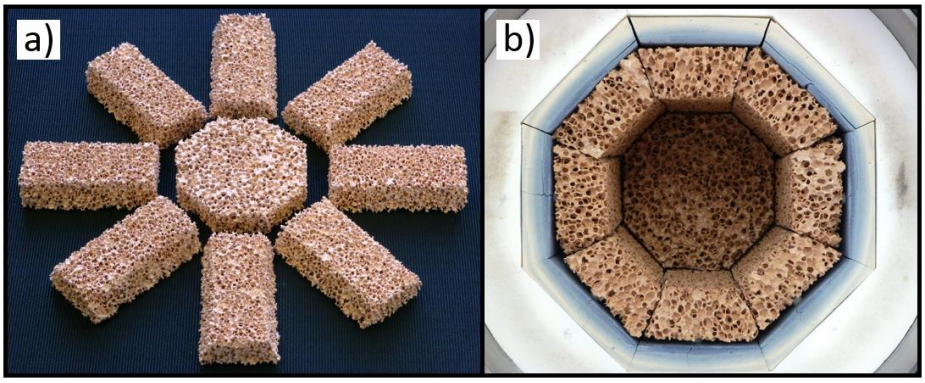

Figure 11: a) RPC parts for new reactor consisting of 8 brick elements and 1 octagonal backplate; b):RPC mounted in octagonal shape inside cavity receiver.

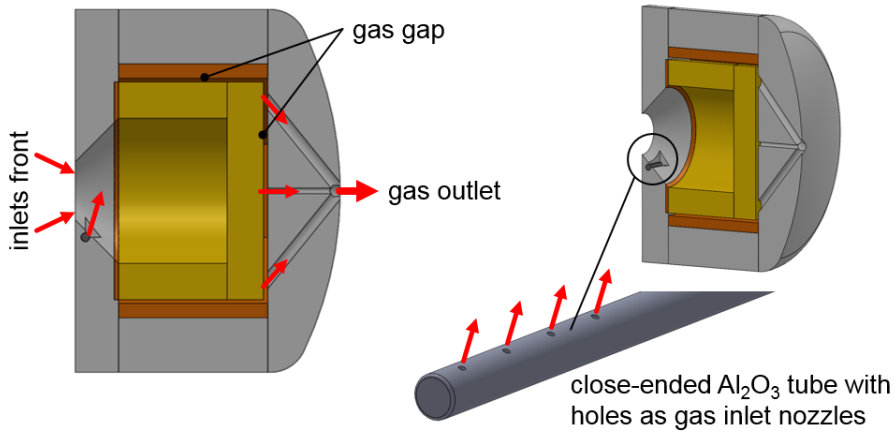

Figure 12: Gas inlet and outlet ports of the 2nd-generation solar reactor design.

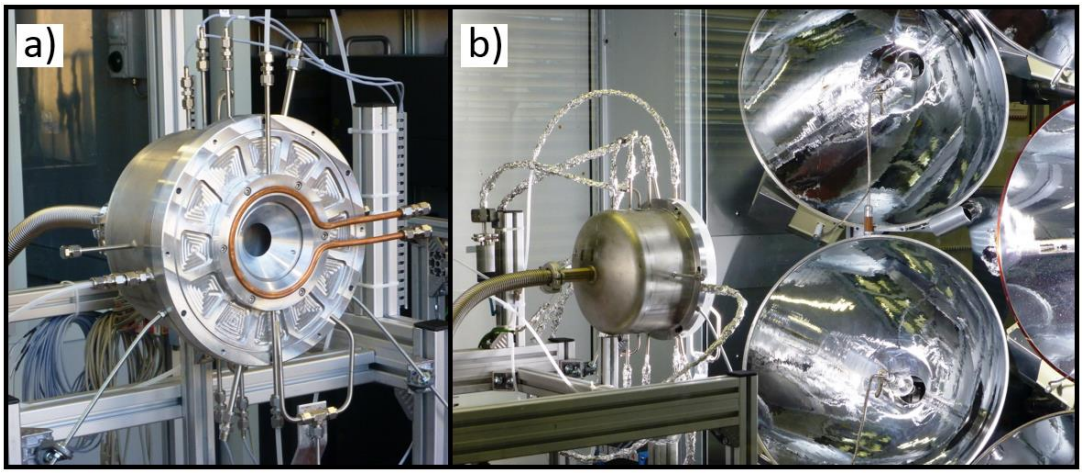

Figure 13: Photographs of: a) the solar reactor; b)the experimental setup at ETH's High-Flux Solar Simulator

Figure 14 (a) shows the nominal solar reactor temperature and O_2, CO and H_2 evolution rates during a typical H_2O and CO_2 co-splitting cycle obtained with the gen 2 reactor. Figure 14 (b) shows the gas concentrations of the product gas stream exiting the reactor of the same cycle. Oxygen, hydrogen and carbon monoxide peak rates were 0.29, 0.37 and 0.15 L min^{-1}, respectively. The absolute amounts of O_2, H_2 and CO released were 2.29, 2.77 and 1.44 L, respectively. The H_2:CO molar ratio was 1.93 and the cycle average syngas concentration 46.4%. The rest is unreacted CO_2 and argon. The syngas composition is very similar to the composition obtained with the first solar reactor prototype for which it was shown previously that the syngas was suitable for liquid fuel synthesis via the Fischer-Tropsch synthesis. Note that with the gen-2 reactor this syngas composition was achieved without stabilizing the oxidation temperature with a low solar power input as it was done previously. The solar-to-fuel energy conversion efficiency was 1.74%. Cycles at conditions which allow achieving higher efficiencies are presented in the next section.

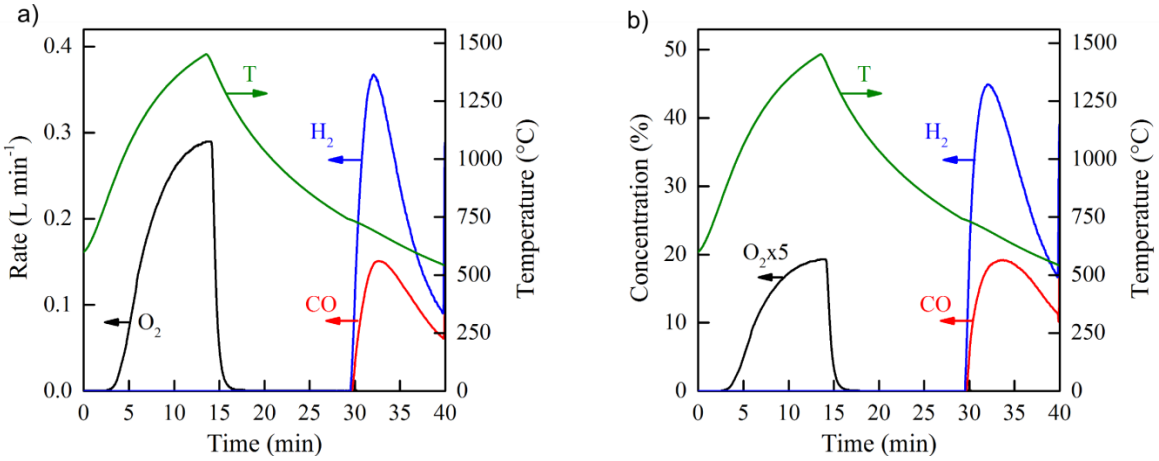

Figure 14: (a) Nominal solar reactor temperature and O_2, H_2 and CO evolution rates during a syngas production cycle. Part (b) shows the nominal reactor temperature and the O_2, H_2 and CO concentration in the product gas stream of the reactor.

Comparison of performance to previous reactor

The benefits of the gen-2 reactor vis-à-vis gen-1 reactor are clearly seen when comparing experimental results under similar experimental conditions. Figure 15 shows the nominal reactor temperature and O_2 and CO evolution rates during CO_2-splitting redox cycles obtained with the gen-1 reactor (dashed lines) and with the gen-2 reactor (solid lines). A summary of the operating conditions for both reactors are listed in Table 1.5. During the initial phase of the solar reduction step at low temperature, the gen-1 reactor shows higher heating rates than the gen-2 reactor with peak heating rates of 184 and 127 °C min^{-1} for the gen-1 and gen-2 reactor, respectively. This is explained by the 82% higher mass loading of ceria in the gen-2 reactor. At elevated temperatures above 1250 °C the heating rates of the gen-2 reactor surpass the heating rates of the gen-1 reactor despite the much higher mass load, yielding average heating rates of 58.5 and 75.5 °C min^{-1} for the gen-1 and gen-2 reactor, respectively. This impressive improvement presumably resulted from decreased re-radiation losses, decreased conduction losses and more uniform flux distribution over the RPC surface. Thanks to these improvements, the solar-to-fuel energy conversion efficiency was increased by 77% from 1.58% with the gen-1 reactor to 2.79% with the gen-2 reactor. Note that the sensible heat of the hot gaseous products exiting the solar reactor or of the RPC undergoing a temperature swing between the redox steps was not recovered. Heat recovery will be addressed in the follow-up project.

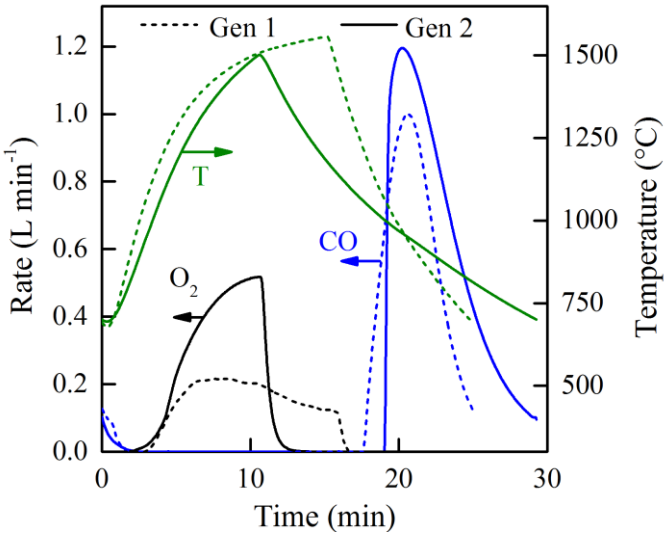

Figure 15: Nominal solar reactor temperatures and O_2 and CO evolution rates during CO_2-splitting redox cycles performed with the gen-1 (dashed lines) and gen-2 reactor (solid lines) with same Psolar = 3.8 kW and individually optimized conditions for each reactor.

To study the stability of the reactor and the reactive structure, 5 subsequent cycles under the conditions were performed with the gen-2 reactor. The resulting temperatures and O_2 and CO evolution rates are presented in Figure 16. Stable performance without measurable degradation was observed during these cycles.

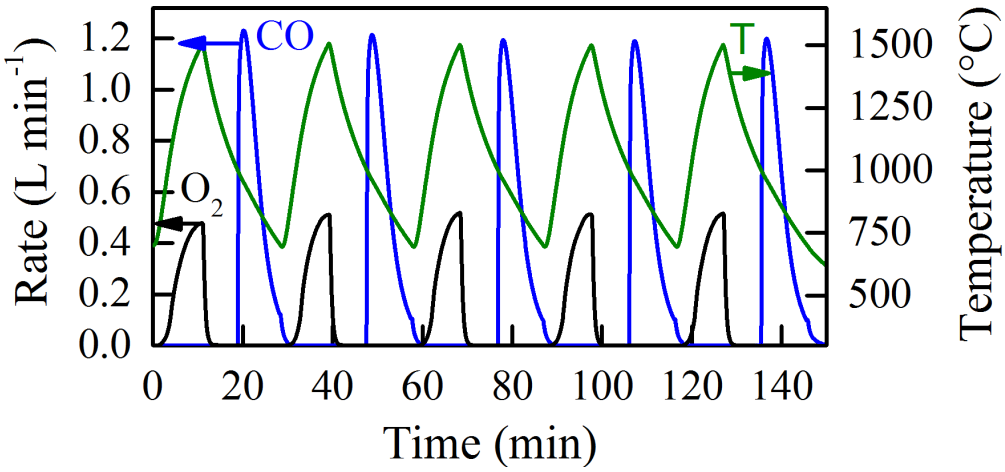

Figure 16: Nominal solar reactor temperatures and O_2 and CO evolution rates during CO_2-splitting redox cycles performed with the gen-2 reactor with experimental conditions chosen for high efficiency.

References:

1. Furler, P., Scheffe, J. R. & Steinfeld, A. Syngas production by simultaneous splitting of H2O and CO2via ceria redox reactions in a high-temperature solar reactor. *Energy Environ. Sci.* **5,** 6098 (2012).
2. Haussener, S., Coray, P., Lipinski, W., Wyss, P. & Steinfeld, A. Tomography-Based Heat and Mass Transfer Characterization of Reticulate Porous Ceramics for High-Temperature Processing. *J. Heat Transfer* **2009,** 23305 (2009).
3. Haussener, S. & Steinfeld, A. Effective Heat and Mass Transport Properties of Anisotropic Porous Ceria for Solar Thermochemical Fuel Generation. *Materials (Basel).* **5,** 192–209 (2012).
4. Chueh, W. C. & Haile, S. M. A thermochemical study of ceria: exploiting an old material for new modes of energy conversion and CO2 mitigation. *Philos Trans. A Math Phys Eng Sci* **368,** 3269–3294 (2010).
5. Haering, H.-W. *The air gases nitrogen, oxygen, and argon*. *Ind. Gases Process.* (Wiley-VCH, 2008). doi:10.1002/9783527621248.ch2

6. Roeb, M. *et al.* Operational strategy of a two-step thermochemical process for solar hydrogen production. *Int. J. Hydrogen Energy* **34,** 4537–4545 (2009).
7. Diver, R. B., Miller, J. E., Allendorf, M. D., Siegel, N. P. & Hogan, R. E. Solar Thermochemical Water-Splitting Ferrite-Cycle Heat Engines. *J. Sol. Energy Eng.* **130,** 41001 (2008).
8. Schunk, L. O. *et al.* A receiver-reactor for the solar thermal dissociation of zinc oxide. *J. Sol. Energy Eng. Asme* **130,** (2008).
9. Perkins, C., Lichty, P. R. & Weimer, A. W. Thermal ZnO dissociation in a rapid aerosol reactor as part of a solar hydrogen production cycle. *Int. J. Hydrogen Energy* **33,** 499–510 (2008).
10. Smestad, G. P. & Steinfeld, A. Review: Photochemical and Thermochemical Production of Solar Fuels from H2O and CO2 Using Metal Oxide Catalysts. *Ind. Eng. Chem. Res.* **51,** 11828–11840 (2012).
11. Chueh, W. C. *et al.* High-flux solar-driven thermochemical dissociation of CO2 and H2O using nonstoichiometric ceria. *Science* **330,** 1797–1801 (2010).
12. Roy, S. C., Varghese, O. K., Paulose, M. & Grimes, C. A. Toward Solar Fuels: Photocatalytic Conversion of Carbon Dioxide to Hydrocarbons. *ACS Nano* **4,** 1259–1278 (2010).
13. Varghese, O. K., Paulose, M., LaTempa, T. J. & Grimes, C. A. High-Rate Solar Photocatalytic Conversion of CO2 and Water Vapor to Hydrocarbon Fuels. *Nano Lett.* **9,** 731–737 (2009).

The research work in WP2 was mostly concerned with modeling the thermochemical reactor. The unsteady 3D fluid flow coupled to radiative, convective, and conductive heat transfers were computed within the cavity-receivers that were successfully tested experimentally by the ETH Zürich.

Firstly, the computational tool was validated using the first-generation geometry (see the computational domain in Figure 17, left). The porous region (RPC) was modeled as a continuum sub-domain characterized by effective properties. A Monte-Carlo approach was used to model the radiative heat transfer within the fluid sub-domain of the computational domain. Large numbers of rays (10^7 in numbers) were traced for their incidence, reflection and absorption within the solar reactor. As no local thermal equilibrium is reached in the porous domain, two energy transport equations were solved, one in the solid and one in the fluid part of the porous sub-domain, with a convective-type boundary conditions. It was shown that the optical thickness of the porous domain is large enough so that radiation can be modeled as a diffusion process (Rosseland's approximation). The computational volumes are of hexahedral structure and the resulting grid consisted of approximately 1.6 million hexahedral cells and approximately 1.7 million nodal points.

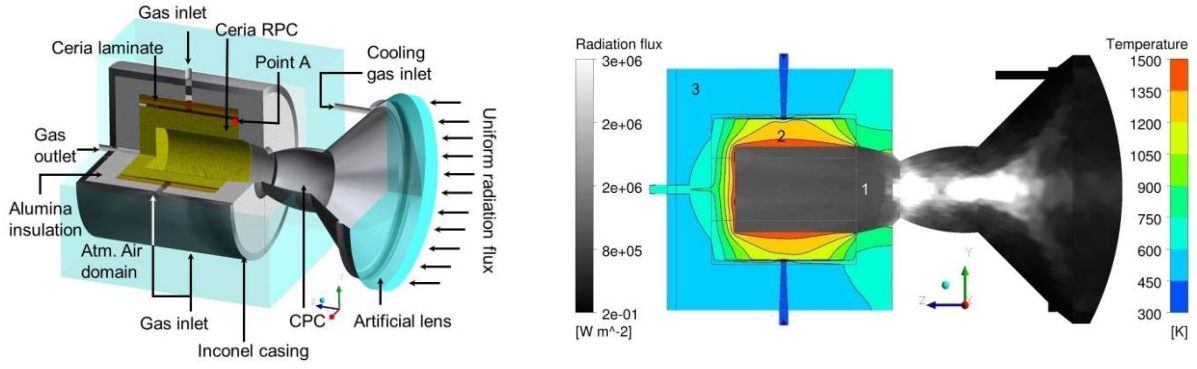

Figure 17: (left) Computational domain for the 1st Generation ETH Zürich cavity-receiver. (right) Temperature field and radiation flux in a cross-plane, 1: cavity, 2: RPC and, 3: Insulation.

The measurement results concerning a pointwise temperature (see Table 1) and heating rate for four different radiative power inputs: 0.8 kW for the pre-heating step and 2.8, 3.4 and, 3.8 kW for the

reduction step were compared to the simulation results.

Power Input [kW]	RPC Temperature [K] *Experiment*	RPC Temperature [K] *Simulation*	Relative error [%]
0.8	1013	1010	-0.3
2.8	1693	1757	+3.8
3.4	1803	1914	+6.1
3.8	1873	2007	+7.1

Table 1:Comparison of measured and simulated temperatures recorded at Point A (see Figure 17 left)

The agreement with measured values is good. Actually, the relative error for the pre-heating stage (P=0.8 kW) is very low. Moreover, considering the fact that single point temperature measurements were performed during an actual CeO_2 reduction step and that this reaction, which is slightly endothermic (dependent upon local temperature and O_2 partial pressure) is not modeled, the systematic error in the direction of over-predicting the local temperatures for all three power inputs is consistent and very satisfactory (see last column of Table1). Similar agreement was obtained concerning the heating rates comparison. From Figure 18 it can be further noticed that in both the experiments and in the simulations the temperature values have not reached their respective plateaus. Furthermore, there is a gradual decrease in the heating rates and the temperatures tend towards reaching asymptotic values. The simulations will help in optimizing the duration of the reduction step so that maximum solar-to-fuel efficiencies are reached.

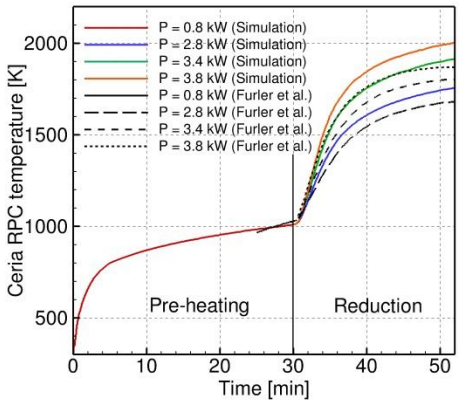

Figure 18: Timewise evolution of the temperature probd at point A in Figure 17 (left). Comparison bewtween the experimental measurements and the numerical results (without reduction reaction modeled).

Secondly, an improved geometry (see Figure 19) provided by the experimental team at ETH Zürich was computed. The expected improvements, in particular in terms of peak temperature reduction and re-radiation losses reduction were predicted by the numerical simulation. Also, the more uniform temperature distribution within the improved cavity-receiver led to higher volume percentage of the RPC reaching the threshold temperature (1500 K), which is beneficiary to the reduction step. An increase in reactor efficiency had been thereby expected and was experimentally demonstrated.

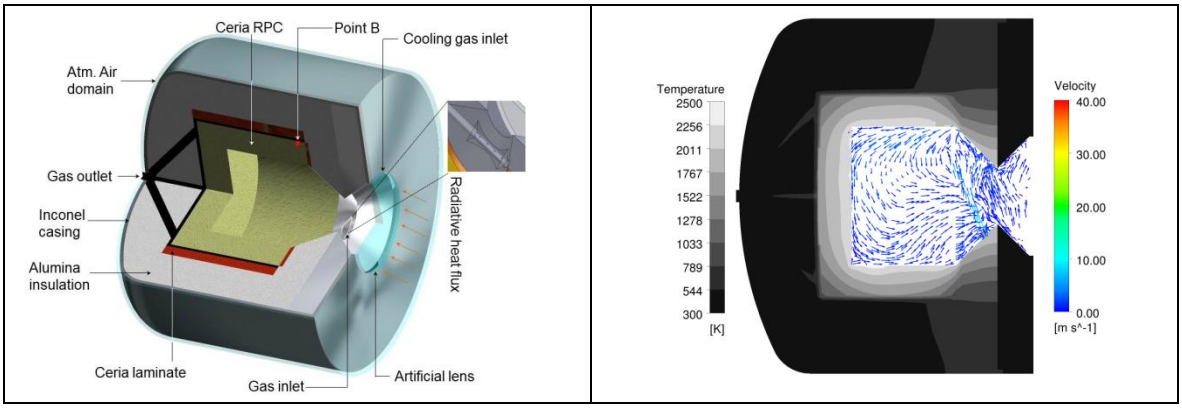

Figure 19: (left) Computational domain of the second generation cavity-receiver. (right) temperature contour plot (grey-scale) and velocity vectors within the cavity.

Analysis based on the numerical simulations provided additional information which is not accessible from the experimental investigation. In particular, concerning the temperature gradients. In the first generation reactor, for a power input of 3.8 kW, the maximum computed RPC temperature is 2592 K and the minimum temperature is 723 K. This temperature difference happens within 0.02 m of RPC's thickness, which results in high temperature gradients and may lead to very high thermal stresses in the RPC structure. The temperatures reached within the second generation reactor after a time of 52 minutes are lower than that of the previous reactor. However, the temperature distribution within the new RPC section (Figure 19) is now more uniform in comparison to that in the pre-optimized reactor. These are the main motivation behind the optimization process, in which the objectives are to reduce the peak temperatures, thereby reducing the heat loss to the environment and the need to avoid sharp temperature gradients within the RPC. The convective heat transfer (see Figure 19 right) can also be optimized using the computational tool proposed in the project.

Concerning the heat balance (see Figure 20), for a radiative power input of 3.8 kW, in the second generation reactor an average of 14.8% of the input energy is used to heat up the ceria RPC, while in the previous reactor it was around 7.6%. Most of that energy is transferred to the insulating layers: 40 % to the alumina insulation, 12% to the inconel wall, and 4% to the ceria laminate. Only about 12% is lost due to natural convection at the outside walls. One of the major advantages in the improved reactor is the reduction in the re-radiation loss, which is helped by the reduction in the peak temperatures within the RPC and also due to the design changes, which introduce changes in the view factors to decrease re-radiation. As compared to the previous reactor, the second generation reactor is designed to have a more uniform temperature above 1500 K. Also, it has less RPC volume above 2000 K.

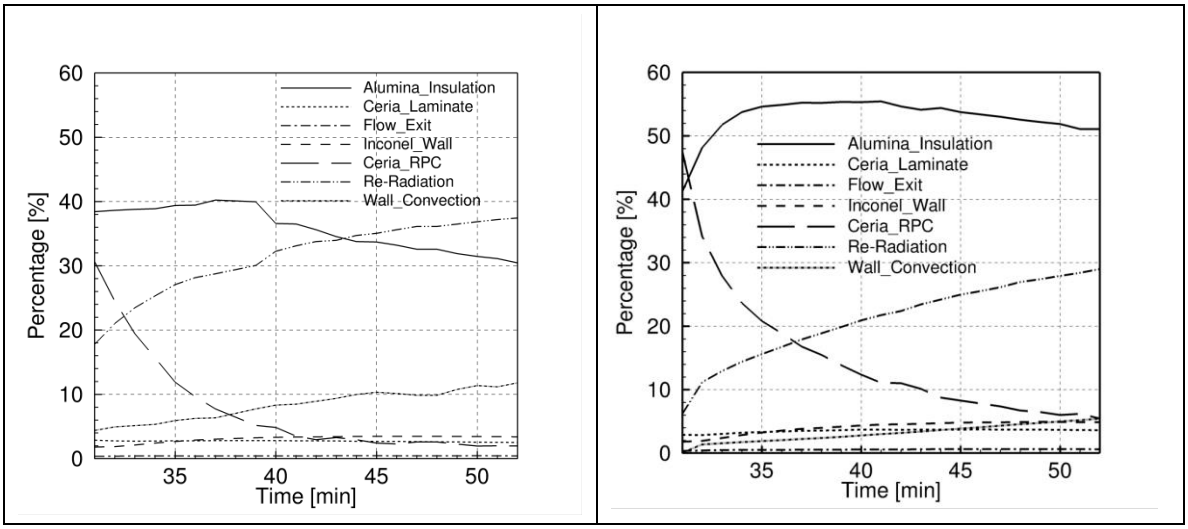

Figure 20: Heat balance for the 1st generation (left) and 2nd generation (right) cavity-receiver geometries. Both computed for a radiative power input equal to 3.8 kW.

Finally, the improved geometry was numerically scaled up (aperture diameter 3.7 times bigger, which yields a RPC volume 50 times larger) and computed with a radiative power input of 50 kW (~13 times the lab-scale power input). As expected, pre-heating and reaction times should be adjusted when using a scaled up configuration. In-field tests one should have a proper on-line diagnostics to ensure that not only a threshold temperature has been reached (e.g. 1500 K) but also that a certain degree of volume homogeneity within the RPC volume has been reached.

The objective of the SolarJet project is to demonstrate and further develop a specific solar energy driven route to convert CO_2 and water into kerosene. The process consists of two main steps, which are essentially independent.

1) In the first step synthesis gas (syngas), a mixture of CO and H_2, is produced from CO_2 and water. This reaction is endothermic and a significant input of energy is thus required. In SolarJet, the sun provides the energy to drive the production of synthesis gas. The specific technology comprises a thermochemical cycle which employs concentrated solar radiation. This technology is being developed at the ETH Zurich and is currently in the research phase.

2) The second step comprises the synthesis of fuels (including kerosene) from synthesis gas. The technology required is available on commercial scale and as such no dedicated development is required. Synthesis gas can be produced from a number of resources including gas, coal and solar energy and through a number of different processes. For its conversion to fuels it is irrelevant through which process the synthesis gas was produced.

The preferred process to convert syngas into kerosene is an application of the Fischer-Tropsch synthesis followed by hydrocracking of the Fischer-Tropsch product. This process, which is applied by Shell in Qatar, yields a mixture of middle distillates including naphta, kerosene and diesel. Depending on the severity of the hydrocracking operation up to approximately 50 w% of the total product can be

qualified as kerosene. The purpose of the work is to check whether the ‘solar syngas’, as produced by the ETH can be used in the standard fuel synthesis process. A 5 litre bottle (p=150 bar) with solar synthesis gas was produced by the ETH and transported to the Shell laboratories in Amsterdam. The composition of this synthesis gas was measured and found to be suitable for the Fischer-Tropsch synthesis. The reaction was subsequently carried out in a standard laboratory scale unit. Figure 21 shows the products (a solid wax and a liquid) as collected from this experiment.

Figure 21: The light (left bottle) and heavy (right bottle) product produced during the Fischer-Tropsch run with the synthesis gas produced by the ETH. The heavy product is a solid white wax. The liquid product consists of mainly water with a thin layer of liquid hydrocarbons floating on it.

Hydrocracking is the final step that converts Fischer-Tropsch wax (the heavy product in Figure 21) into kerosene and other middle distillates like diesel and naphta. Whereas the amount of synthesis gas produced by the ETH was sufficient to be converted in a standard Fischer-Tropsch experiment, the amount of wax produced in this experiment is clearly below what is required for a standard hydrocracking experiment. This implied that a dedicated reactor and procedure had to be designed for the purpose of the Solar Jet project. To avoid the technical risks of this operation as much as possible it was decided to downscale the hydrocracking experiment to such an extent that only a relatively small fraction of the wax produced in the Fischer-Tropsch run would be required to perform the experiment. This small scale hydrocracking experiment yielded a yellowish liquid, a picture of which is shown in Figure 22, The yellow colour is an indication for the presence of some olefins, which can be removed by additional hydrogenation.

Figure 22: The liquid product produced after hydrocracking the Fischer-Tropsch wax (the heavy product shown in Figure 21).

The composition of the liquid product was obtained through a standard 'simulated distillation' and table 2 gives a breakdown in terms of middle distillate fractions. According to the Jet A fuel standard (http://www.etc-cte.ec.gc.ca/databases/Oilproperties/pdf/WEB_Jet_A-Jet_A-1.pdf), the kerosene fraction of the liquid product is 35.6 wt%.

Table 2: The composition of the liquid product

	Boiling range	**Mass fraction**
Naptha	0-145 ^{o}C	17.1
Kerosene	145-300 ^{o}C	35.6
Gasoil	300-370 ^{o}C	17.1
Heavier than gasoil	>370 ^{o}C	30.2

It has been firmly proven that synthesis gas produced through the solar thermal process route, currently under development at the ETH Zurich, is suitable for conversion in the combined Fischer-Tropsch / hydrocracking process. A small amount of solar kerosene has been produced in the experiments. It can be concluded that the basic premise of the SolarJet project is technically sound.

This result is not surprising as the synthesis gas produced by the ETH did not contain impurities that would be detrimental to the catalysts employed in the conversion process. Naturally, any other (solar driven) process that produces synthesis gas could be coupled to existing Fischer-Tropsch/hydrocracking technology to yield liquid hydrocarbon products.

The main results are presented in the following sections:

- State-of-the-art of process steps and maturity gates
- Overall energy conversion efficiency and specific yield
- Area requirements and geographical potential
- Ecological performance
- Production cost

State-of-the-art of process steps and maturity gates

The cycle of fuel production and use is shown in Figure 23. Direct solar energy is concentrated to provide high temperature heat to drive a two-step thermochemical cycle based on redox reactions of cerium oxide. Carbon dioxide and water are split to produce syngas which can further be converted to liquid hydrocarbons via the Fischer-Tropsch process. Fischer-Tropsch synthesized fuel is certified for aviation. When carbon dioxide is captured from the atmosphere, the material cycle can be closed which leads to a sustainable jet fuel production process.

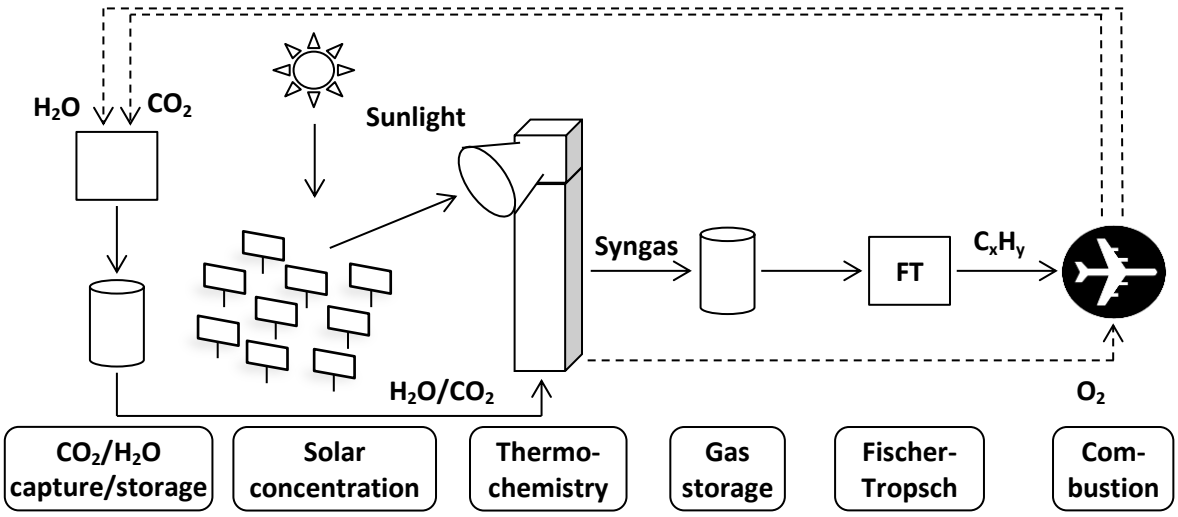

Figure 23: Production path of carbon-neutral SOLAR-JET fuel

Concentration of solar energy

Concentration of solar radiation is a commercialised technology in the field of concentrated solar power (CSP) for electricity generation. Of the different concentration techniques which are commonly used in CSP applications, only point focus devices are capable of delivering concentration ratios high enough to achieve adequate temperatures to drive the thermochemical cycle. A solar tower power plant can concentrate sunlight by a factor of 1000-1500 (Meier & Sattler, 2010) while a dish system can deliver even higher concentration ratios which may lead to a higher overall efficiency since a higher power density helps reduce reradiation losses from a reactor. However, due to constructional constraints, single dish devices can only reach a certain power level whereas the scalability of a tower power plant allows to reach higher power levels in a single reactor. It can be assumed that for a larger reactor, heat losses through radiation, conduction and convection can be further reduced due to its enhanced volume-to-surface ratio.

From theoretical analyses, further improvements in efficiency seem possible, however, as the technology is already almost mature, a reduction of the specific cost has a high priority. The recent development includes autonomous heliostats that communicate wirelessly with the control room and that offer a reduction of field wiring. Heliostats could be made more cost effective through a reduction of the weight of the support structure which could be achieved by polymeric films that reduce the weight of the reflective area or by wind fences that reduce the wind force on the heliostat field. Solar dishes which are likely to have higher specific production costs due to their more complex construction could benefit likewise from a reduction of the weight of the support structure, e.g. by using composite materials and by using processes otherwise used in industry.

Concentration of sunlight requires cost optimization in order to reach values of 120 $/m² and 100 $/m² for the demonstrator and the first commercial plant, respectively.

Thermochemical conversion

The thermochemical conversion has been identified to have the potential for further efficiency improvements. Recent developments of the reactor technology include concepts for heat recuperation from the gas and the solid phase, the use of a vacuum pump to decrease the oxygen partial pressure more efficiently and the research of new reactive materials with lower energy requirements and that allow using lower temperatures during reduction. At ETH, the increase of the specific surface area of porous ceria through the introduction of dual-scale pores enables considerably higher oxidation rates and thus the production of syngas with a higher purity.

CO_2 capture

For the production of solar syngas, CO_2 is required which may be supplied either from point sources or by capture from the air. In a **short- to mid-term perspective**, CO_2 can be captured from point sources by pre-combustion capture, post-combustion capture, oxyfuel combustion, or capture from other industrial processes. As CO_2 is an abundant product of many commercial processes with little demand, the supply is secured at costs of roughly 10-50 $/$t_{CO2}$.

However, from an ecological point of view, in the **long-term perspective**, capture from the air is a more suitable option. Also here, different technological options exist depending on the nature of the capture process. In the development of carbon dioxide capture from air, progress has been made through a decrease of the energy requirement. First demonstration plants are being installed in Canada by Carbon Engineering and in Switzerland by Climeworks with capture performances on the order of 1000 tons per year. While this is a promising development, further improvements and scale-up are required for the implementation at a scale of a potential SOLAR-JET plant.

A cost efficient scale-up of CO_2 extraction from renewable sources is required for the long-term provision of sustainable solar fuel for which technologies are still at low TRL.

H_2O provision

Besides carbon dioxide, water is one of the resources required as an input to the process. As the fuel

production plant is likely to be located in arid regions to take advantage of the high solar irradiation, natural fresh water resources may not be in the close vicinity. It has therefore to be supplied to the site either by concurrent capture from air with CO_2 or provided by pipeline transport from the sea. Among the common seawater desalination technologies, reverse osmosis was determined to be the most energy efficient at demonstrated values of 1.8 kWh/m³. The water then has to be transported to the plant site which requires energy for pumping. For a plant location of 500 km off the coast and at 500 meters altitude, the energy for pumping is one order of magnitude larger than for desalination. In total, the energy requirement is less than one percent of the energy stored in the fuel. The costs of 1000 liters of freshwater are on the order of 0.5 $. At a water requirement of ~ 5 L/L_{fuel}, water provision only slightly influences the production costs. Seawater desalination and subsequent water transport is thus seen to play a minor role in the overall energy budget and plant economics.

Fischer-Tropsch conversion

The conversion of syngas into liquid fuels with the Fischer-Tropsch process is technologically mature and economically viable on a very large scale as shown by e.g. the Shell Pearl GTL plant in Qatar. Depending on the desired product mix, different catalysts and temperature levels are used. For the production of longer-chained hydrocarbons such as kerosene, a low-temperature process with a Cobalt-based catalyst is used. In principle, the reactor technology is scalable also to lower production volumes, however, the economics of Fischer-Tropsch plants currently require a minimum size of about 1000 barrels of liquid product per day. Recent development comprises also small-scale facilities for gas sources at oil fields which convert otherwise flared gas into liquid products. This will benefit also the SOLAR-JET production path, as economic small-scale Fischer-Tropsch units will give a larger technological and economic flexibility to a possible plant implementation. Also the development of intermittently operated FT units that run economically and in a robust way are of interest for the future implementation of the SOLAR-JET technology.

Integration of process steps in centralized plant

In the present project, a decentralized laboratory validation of the SOLAR-JET technology has been achieved. Towards implementation, both an integrated solution in a relevant environment and a scale-up of the reactor technology for further efficiency enhancements should be pursued.

For a **demonstration plant**, a single dish or small tower system is foreseen as the concentrator. At this power level, the required input of water and (compressed) carbon dioxide is on the order of a couple of liters per day which can easily be supplied by gas bottles and small liquid storage tanks. There will most certainly be no dedicated water desalination or carbon dioxide capture stage at this point. Equally, the FT unit could be similar to existing research facilities that converts the produced and stored synthesis gas into fuels. The main challenge is therefore the scale-up of the thermochemical reactor to a power level of 30-100 kW_{th} and its integration with the concentrator. The produced synthesis gas needs to be stored at a rate of about 15000 liters or several compressed gas cylinders per day.

For a first **commercial plant**, a size of about 1000 bpd is foreseen which corresponds to about 30000

dishes or about three towers. A dish system would probably use a centralized gas storage and FT unit which requires complex piping to connect each of the reactors to the storage devices for resources and products. System integration therefore needs to connect all of the process steps in an efficient manner not only to show technological but also economic viability. In addition purge gas separation and potentially other gas separation units need to be integrated in the facility.

Table 3: Maturity levels of SOLAR-JET process steps and of their integration into the overall production cycle.

Process step	Maturity	TRL
Concentration	Industrial application	9
CO_2 capture	Demonstration plants	6
H_2O provision	Industrial application	9
Thermochemistry	Lab-scale	3
Fischer-Tropsch	Industrial application	9
Gas management	Industrial application	9
Fuel management	Industrial application	9
Integration of production path	Lab-scale	≤3

Overall energy conversion efficiency and specific yield

For a baseline case of a solar stand-alone facility with an output of 1000 bpd of jet fuel and 865 bpd of naphtha as a by-product, an overall energy conversion efficiency of 5.0% is derived. The overall efficiency is defined as the energy content of the hydrocarbon fuel product (LHV) referenced to the solar resource (DNI) which is incident on the mirror area. The overall energy conversion efficiency needs to be reduced by a land-use factor in order to obtain an efficiency related to land requirement. With an assumed land-use factor of 25% (reflector aperture area devided by land area) one obtains an **area specific energy conversion efficiency of 1.1%.**

The specific yield of a solar fuel facility at a particular location is given by the annual solar resource multiplied by the area efficiencies. The expected yield at an exemplary DNI of 2500 kWh/(m^2·yr) is 28 kWh/(m^2·yr) of hydrocarbon fuel, corresponding to 14,000 liter/(ha·yr) of jet fuel and an equal share of naphtha as a by-product.

It is important to note that the theoretical potential for the overall energy conversion efficiency of SOLAR-JET fuel is well beyond 10%. Assuming an energy conversion efficiency according to the thermodynamic potential for solar thermochemical syngas production of 30% (Furler, Scheffe, Gorbar, Moes, Vogt, & Steinfeld, 2012), a solar concentrator efficiency of 80% (dish concentrator) and a FT conversion efficiency of 70% results in a total energy conversion efficiency above 15%.

Area requirements and geographical potential

In order to evaluate the production potential for solar thermochemical jet fuel, we re-evaluate a GIS

based analysis by DLR for CSP electricity (2012) using the SOLAR-JET area-specific fuel yield, i.e. the CSP electricity production potentials which were evaluated assuming an area-specific yield of 4.5%, are rescaled by a lower area-specific yield of solar jet fuel production of 0.56%.

Europe

The solar thermochemical fuel production potential is 110 Mtoe/yr, which exceeds the EU-28 final energy consumption of air transport of 50.2 Mtoe in 2011 (Eurostat, 2013). Thus, a 100% substitution of the current EU-28 jet fuel demand is in line with the EU-27+ geographical production potential of solar thermochemical fuel.

World

Very attractive conditions for concentrated solar energy technologies are found in different places in the world. A global solar thermochemical fuel potential of 32000 Mtoe or about 125 times the global aviation fuel demand in 2012 is calculated. This enormous geographical production potential implies that land use change is small as solar thermochemical jet fuel production will not be employed close to its geographical production potential. Instead, solar-thermochemical fuel production can be located with respect to socio-economic and environmental criteria such as DNI level, feedstock supply, existing infrastructure, cost of capital, available work force, biodiversity etc. Viewed exclusively in terms of geographical production potential one can easily achieve 100% substitution of conventional jet fuel even at considerably lower area-specific yield. This relaxes the efficiency requirements for the introduction of solar thermochemical fuel in terms of production potential. Instead, the efficiency requirement should primarily reflect economic and environmental considerations rather than geographical production potential.

Ecological performance

Greenhouse gas emissions are defined as the indicator of ecological performance for SOLAR-JET fuel production. For carbon dioxide capture from the air, potentially very low GHG emissions are possible, making the fuel pathway an environmentally friendly alternative to conventional jet fuel. For a production plant with a capacity of 1000 bpd of jet fuel and 865 of naphtha, GHG emissions of 0.5 $kg_{CO2\text{-}equivalent}$ per liter of jet fuel are estimated. Key drivers of the ecological performance are the emissions associated to the solar concentration facility and the origin of CO_2 and electricity used in the process.

Production costs

The production costs of SOLAR-JET fuel are strongly driven by the large investment costs required for the solar concentration facility, its operation and maintenance costs, CO_2 capture, and electricity costs. Depending on the operation mode of the production plant and assumptions about the state of the art of thermochemical efficiency and capital costs, an economically interesting production scenario can be created. For a plant size of 1000 bpd of jet fuel, production costs of 2.2 € per liter are estimated.

1.4 Potential Impact

1.4.1 Socio-economic Impact

The **socio-economic impact** of large-scale production of SOLAR-JET fuel is expected to be two-fold, energy supply security and wealth from local fuel production. The potential to reduce the dependency of oil producing countries for the supply of hydrocarbon fuels and thus to establish supply security is a strong driver for high-insolation regions such as in southern Europe, Africa and Australia. Due to the large solar resource and the wide availability of the resources water and CO_2, single countries have the potential to cover their own demand of jet fuel and some of them even the global demand.

The SOLAR-JET technology requires a large solar resource of direct normal insolation (DNI) which is typically found in countries with vast areas of arid non-arable land. The construction of large-scale production facilities could therefore **bring wealth to economically challenged regions** and help to develop local industries and economies. As this is a new technology, it would not replace an existing industry but would be complementary and therefore create new jobs and opportunities. It is conceivable that the construction of a SOLAR-JET plant with its necessary water provision could supply a surplus of fresh water to the local population and agriculture with a profound and sustainable positive socio-economic impact.

An economic model is used for the **estimation of jet fuel production costs**. A baseline case with a plant size of 1000 bpd of jet fuel production is chosen. At the same time, 865 bpd of naphtha are produced from the same facility. The solar-stand alone facility, i.e. without external sources of heat or electricity, is publicly financed and located in a region with 2500 kWh/(m² a) of direct normal irradiation with a tower system as concentrator. Thermochemical energy conversion efficiency is assumed to be 20%. Carbon dioxide is provided by an air capture unit located onsite and water by seawater desalination located at 500 km distance and 500 m altitude difference. The produced fuels are transported over 500 km via pipeline.

For the calculation of jet fuel production costs from the baseline plant, investment costs and operation and maintenance costs (O&M) are estimated. The total investment costs are 880 million € for the fuel production plant, where 74% are for the heliostat field, 11% for the thermochemical reactors including the reactive material ceria, 8% for the solar tower, 5% for the Fischer-Tropsch conversion unit, and smaller contributions for buildings and other technical equipment. The O&M costs are 123 million € per year, where 37% are for operation and maintenance of the heliostat field, 32% for CSP electricity, 27% for CO_2, and minor contributions for the operation and maintenance of the Fischer-Tropsch unit, water provision, mirror replacement, and fuel distribution.

The annuity method is used for the derivation of production costs of jet fuel. At first, the present value of the O&M costs are calculated as the annual O&M costs multiplied with the annuity factor, where the O&M costs are in constant currency and the annuity factor is calculated with the real interest rate. Naphtha is sold at a fixed price of 80% with respect to the jet fuel production costs. The lifetime of the publicly supported plant is 25 years and the interest rate is nominal 6% for the

baseline case. Public funding could be the case if such a facility is supported by the government in order to secure supply security of liquid hydrocarbon fuels.

Production costs of 2.2 € per liter of jet fuel are estimated. For the present case, the economics of the plant are ruled by the accumulated O&M costs which have about twice the impact with respect to the investment costs. However, plant economics are also strongly driven by investment costs, as the concentration of the solar resource requires an expensive infrastructure.

In order to study the influence of a set of variables, a sensitivity study is performed for the level of solar irradiation, thermochemical efficiency, life time of the plant, specific investment costs of reflective area, and costs of CO_2 provision. An improved plant location that increases the level of solar irradiation by 10% reduces the production costs by 4.7%. Similarly, a reduction in solar irradiation by 10% increases production costs by 5.8%. These values are not identical because the increase by 10% of solar irradiation diminishes the heliostat field by 9%, while its decrease requires a larger reflective surface area of 11%. The same is true for the variation of thermochemical efficiency that defines the required size of the heliostat field: an increase of efficiency by 10% reduces the production costs by 6.1%, while a similar decrease in efficiency leads to an increase by 7.5%. As for the concentration of dilute solar energy a large field of mirrors is needed, investment costs for solar concentration play a major role. A variation of ±10% of the unit cost of heliostat area leads to a variation of production costs of ±2.4%. The 10%-reduction in lifetime of the plant increases the production costs by 5.0%, while a 10% longer lifetime reduces the costs by 4.0%. Finally, the costs of CO_2 provision have the smallest influence of ±1.8% on the production costs. Solar irradiation, thermochemical efficiency, and plant lifetime are thus identified to have the largest influence on plant economics and are consequently the main cost drivers of the process.

1.4.2 Wider Societal Implications

Climate impact

A **life-cycle analysis is performed** for a baseline case of a fuel production plant of 1000 bpd output of jet fuel to estimate the global warming potential associated to jet fuel and naphtha. The functional unit is 1 L of jet fuel, where 0.87 L naphtha is produced as by-product. A well-to-wake boundary is chosen that includes resource provision, concentration of solar energy, thermochemistry, and Fischer-Tropsch conversion, as well as final combustion of the fuel. As CO_2 is captured from the air, the amount of CO_2 in the atmosphere is reduced in the capture process which counts negatively in the overall CO_2 balance. The plant operates in a solar stand-alone configuration, i.e. all heat and electricity requirements are covered by the local conversion of solar primary energy.

Life cycle greenhouse gas emissions are 0.49 $kgCO_2$-eq. per liter jet fuel and 0.55 $kgCO_2$-eq. per liter naphtha. Largest influences on the positive emissions have fuel combustion with 65%, FT conversion with 16%, and construction, use and decommissioning of the solar concentration facility with 12%. Emissions of the FT conversion originate from the combustion of the light hydrocarbon

fraction in a combined heat and power plant, as well as fugitive emissions. Emissions of the solar concentrator are almost completely associated to its construction and deconstruction, while its use has only a small influence. Only small contributions are due to the thermochemical reactors, electricity, and fuel transportation. Greenhouse gas emissions could be reduced by about 80% through the use of solar jet fuel compared to conventional jet fuel. This significant savings potential is well below current reduction threshold of 35% and even the stricter emissions reductions targets set by the EU for the use of biofuels.

The solar stand-alone configuration has low greenhouse gas emissions because heat and electricity is provided by conversion of solar primary energy. Grid electricity that is partly based on fossil energy carriers is thus not used. Also capture of carbon dioxide from the air significantly reduces the emissions compared to the capture from fossil sources if the fossil emissions are included into the system boundaries. Different plant configurations are possible, where also the heat and power from the combined heat and power plant is supplied by renewable energy conversion, thereby further reducing the emissions.

A sensitivity study is performed on the variables solar irradiation level, thermochemical efficiency, lifetime of the plant, and emissions from the construction, use and deconstruction of the concentration infrastructure, in which selected variables are varied by ±10% at constant output of the plant. The results indicate that a variation of the plant lifetime, of thermochemical efficiency, or of solar irradiation have a similar influence on the overall greenhouse gas emissions: a reduction by 10% of the variables leads to higher emissions by 10-12%, while a 10% increased value deminishes the costs by 8-10%. A longer lifetime distributes the environmental burdens associated with the infrastructure and operation of the plant over a different number of years and thus the specific emissions per unit fuel produced are altered. Solar irradiation and thermochemical efficiency define the required mirror area and thus the emissions associated with their production. The rather large number of mirrors for the concentration of sunlight has an impact also through the associated emission factor per unit of mirror area. A change by ±10% varies the life cycle GHG emissions by ±8.6%. Thus, there is a possible improvement through a decrease of the material intensity of the heliostats, an interesting topic also for economic reasons.

If CO_2 capture from fossil sources were introduced, it would dominate the emissions and show a different sensitivity with respect to the chosen variables. An improvement of the climate impact of solar jet fuel production could therefore be achieved through the choice of a highly irradiated plant location, the enhancement of the thermochemical conversion step, a prolongation of the lifetime of the plant components, and a reduction of the material intensity of the mirrors and the solar tower.

CO_2 reduction potential for complete substitution of jet fuel

The associated CO_2 reduction potential is estimated from the specific greenhouse gas emissions of the SOLAR-JET fuel and the market size of aviation fuel which is currently 254 Mt (2012). If the complete jet fuel demand is supplied by SOLAR-JET fuel, about 805 Mt of CO_2 could be saved.

Benefit for countries with large solar resource

For the production of solar thermochemical fuels, a high direct solar irradiation is required which is mainly found in countries of the Mediterranean region, the Middle East, Australia, and the Southwest of the United States. The implementation of a fuel production infrastructure could therefore lead to significant investments and job creation opportunities in these regions which could help to develop the local and regional economy. In the following, the investments and the number of jobs created are estimated for the establishment of solar thermochemical fuel production.

Future investment opportunities:

Similar to most renewable energy technologies solar thermochemical fuel production has high upfront cost and relatively low annual maintenance and operation cost. The development of production capacity is therefore accompanied by large capital expenditure. A coarse estimate on capital requirement may be derived from the size of the solar field area of $1.3*10^{10}$ m^2, and the specific investment costs of the solar plant. Projected heliostat costs range significantly below 200 $/$m^2$, where this latter value may serve as an upper bound estimate of the total specific financial investment in the n-th solar fuel plant. Multiplying the required collector area with the specific investment cost yields a total investment of 2600 billion $ for the complete substitution of aviation fuel. This number can be compared to the world's gross domestic product (GDP) of about 74,000 billion $ in 2013 (CIA, 2014). Thus less than 1% of the global GDP is required for a capacity roll-out time of one decade.

Future job creation opportunities:

A large scale roll-out of solar thermochemical fuel production capacity would take place in regions with favourable solar resource. It is estimated that $1.3*10^{10}$ m^2 of mirror area are required for a 100% substitution of conventional jet fuel. Assuming an installation period equal to a plant life time of 30 years equates to an annual installation of $4.3*10^8$ m^2 mirror area. The US National Renewable Energy Laboratory lists construction job years and mirror areas for existing CSP solar tower facilities, including Gemasolar (800 job years for 304,750 m^2), Ivanpah (1896 job years for 2,600,000 m^2) and Crescent Dunes (1500 job years for 1,071,361 m^2) (NREL, 2014). The installed mirror area per construction job year varies widely from 381 m^2 for Gemasolar (Spain) to 1370 m^2 for Ivanpah (US). Assuming the larger value of 1370 m^2 per job year, an annual addition of $4.3*10^8$ m^2 mirror area requires 314.000 job years for construction. Although this represents a major work force especially in scarcely populated areas, this work force does not appear as a show-stopper. It may also be expected that the installed mirror area per construction job year will increase due to automation. The required work force for operation and maintenance of concentrated solar thermal facilities is much smaller than for plant construction. In 2010, 446 people were employed for operation and maintenance of Spanish CSP electricity generation, while 23,398 people have been employed for construction (Deloitte, 2011).

1.4.3 Main Dissemination Activities

All dissemination activities performed to promote the project ans its results are listed in the table 2.1.2, which can be found below. They mainly consisted in developing a public website (www.solar-jet.aero) which was kept up-to-date during the whole project implementation and attending events and conferences where the target audience (industry, policy makers, scientific community) could be approach. Also, as shown under the table 2.1.3 below, several scientific publications were issued by partners in the framework of the project. The most successful communication action for the project is considered to be the press release announcing the production of the first world solar kerosene. This gave the project an even greater visibility, attracted new visitors to the public website and was followed by several other dissemination activities such as intervention of the project coordinator at the local radio or publication of articles in the national and international press. Last but not least, the SOLAR-JET project attended the Aerodays 2015 in London to communicate about its final results and future perspectives. The project displayed at its stand the ETH solar thermochemical reactor used for the production of the first “solar” kerosene in 2014 and gave further information about the main results achieved during the project. With a total attendance of about 50 visitors, the project was able to attract high-level officials and representatives of companies engaged in the research of renewable fuels and related technologies. With a scheduled visit of the guided VIP-tour and a proposed feature as a conference article, the attendance of the SOLAR-JET project was judged very positively.

1.4.4 Exploitation of Results

The research performed in the SOLAR-JET project has lead to an important advancement of the theoretical and experimental knowledge in the field of solar thermochemical fuels. The evolution of the solar reactor technology allowed to increase the solar thermochemical energy conversion efficiency about 2.7% which is the highest measured efficiency for CO_2 splitting in a solar device so far in the world. As this was achieved in the laboratory, the technology readiness level currently is 3-4, which precludes product development. However, this significant achievement is a prerequisite for the next step, i.e. the advancement of the technology from the laboratory environment to the field to further increase the efficiency and consequently the likelihood for implementation. In fact, this step shall be performed in the Horizon 2020-project “Sunlight-to-liquid” starting in 2016.

Furthermore, at present, the recent developments including the increase of solar thermochemical energy conversion efficiency in the SOLAR-JET project underline the large theoretical potential that lies within this fuel pathway. In the course of the analyses performed in the project, no fundamental obstacles were identified for the future development of large-scale solar fuel production. This clearly indicates that this pathway should be further investigated including the construction of demonstration plants to advance the technology. On the other hand, it is too early to decide which of the many alternative fuel pathways will be the most promising but the results achieved in the project can be used for decision making in the context of funding assigned to upcoming research

projects.

1.5 SOLAR-JET Consortium

Project consortium			
Project acronym	SOLAR-JET	**Project nr.**	285098
Project scientific coordinator		Dr. Andreas Sizmann	
    			
Beneficiary nr.	**Organization Short Name**	**Address**	**Stakeholders**
1	BHL	**Bauhaus Luftfahrt e.V. (BHL)** Willy-Messerschmitt-Straße 1 85521 Ottobrunn Germany	Dr. Andreas Sizmann Prof. Dr. Mirko Hornung Christoph Falter Dr.Christoph Jeßberger Dr. Valentin Batteiger Oliver Boegler
2	ETH	**ETH Zurich (ETH)** Institute of Energy Technology Sonneggstrasse 3 8092 Zurich Switzerland	Prof. Dr. Aldo Steinfeld Dr. Philipp Furler Daniel Marxer
3	DLR	**Deutsches Zentrum für Luft- und Raumfahrt (DLR)** Institute of Combustion Technology Pfaffenwaldring 38-40 70569 Stuttgart Germany	Dr. Patrick Le Clercq Parthasarathy Pandi
4	SHELL	Solar Fuels team at **Shell Global Solutions International BV** Grasweg 31 1031 HW Amsterdam The Netherlands	Prof. Dr. Hans Geerlings
		Aviation Fuels Development Manager at **Shell Research Ltd** Shell Technology Centre Thornton P.O. Box 1 Chester CH1 3SH United Kingdom	Dr. Joanna Bauldreay
5	ART	**ARTTIC** Elsenheimerstr. 59 80687 München Germany	Dr. Martin Dietz Justine Curtit

2. Bibliography

(2012, September). Retrieved from http://www.nrel.gov/csp/solarpaces/project_detail.cfm/projectID=40

CIA. (2014, July). Retrieved from The World Fact Book: https://www.cia.gov/library/publications/the-world-factbook/

Deloitte. (2011). *Macroeconomic impact of the Solar Thermal Electricity Industry in Spain.*

Eurostat. (2013). *Energy, transport and environment indicators.*

Furler, P., Scheffe, J., Gorbar, M., Moes, L., Vogt, U., & Steinfeld, A. (2012). Solar Thermochemical CO2 Splitting Utilizing a Reticulated Porous Ceria Redox System. *Energy&Fuels*.

Meier, A., & Sattler, C. (2010). *Solar fuels from concentrated sunlight.* PSI.

NREL. (2014). Retrieved from Concentrating Solar Power Projects: http://www.nrel.gov/csp/solarpaces/power_tower.cfm

Stratton, R., Wong, H., & Hileman, J. (2010). *Life Cycle Greenhouse Gas Emissions from Alternative Jet Fuels.* PARTNER Project 28 report, Version 1.2, Partnership for AiR Transportation Noise and Emissions Reduction.